This is to certify that the

thesis entitled

INDEX OF REFRACTION CORRECTIONS FOR LASER DOPPLER ANEMOMETER MEASUREMENTS IN CYLINDRICAL AND CONICAL GEOMETRIES

presented by

Robert Alan Pincus

has been accepted towards fulfillment of the requirements for

M.S. degree in Chemical Engineering

Charles A. Petty

Major professor

Charles A. Petty

Date July 19, 1985

INDEX OF REFRACTION CORRECTIONS FOR LASER DOPPLER ANEMOMETER MEASUREMENTS IN CYLINDRICAL AND CONICAL GEOMETRIES

By

Robert Alan Pincus

A THESIS

Submitted to
Michigan State University
in partial fulfillment of the requirements
for the degree of

MASTER OF SCIENCE

Department of Chemical Engineering

1985

ABSTRACT

INDEX OF REFRACTION CORRECTIONS FOR LASER DOPPLER ANEMOMETER MEASUREMENTS IN CYLINDRICAL AND CONICAL GEOMETRIES

By

Robert A. Pincus

A phenomenon that must be accounted for when using laser doppler anemometry to make local velocity measurements in fluid flow systems is the refraction of the light beams. Corrections for the refraction phenomenon are developed that provide accurate position and velocity information. A parametric study of the variables that affect the refraction corrections is performed to provide insight into the design of good LDA experiments and test sections. Results indicate that refraction-related measurement corrections are affected by the refractive indices of all media through which the light beams pass, the geometry of the test section, and the position of the beams. These corrections can be used to choose test section materials, test fluids, and test section geometry so as to minimize measurement errors.

TABLE OF CONTENTS

LIST OF TABLES

LIST OF FIGURES

NOMENCLATURE

Angles

k	characteristic half-angle of the focusing lens
θ_H	half-angle of the hydrocyclone
θ_{2B}	
$\underset{\sim}{\theta}_{2A}$	angles which describe the paths of the beams relative to the normal vectors of the various interfaces
$\tilde{\theta}_{2A}$	
$\underset{\sim}{\theta}_{3A}$	
θ_{3A}	
θ_A	angle with respect to the optical bisector that describes where the beams intersect the hydrocyclone wall

Vectors describing the path of the light

$\tilde{\underline{l}}_1$, $\underline{l}_1$	vectors describing the path of the light through the first medium
$\tilde{\underline{l}}_2$, $\underline{l}_2$	vectors describing the path of the light through the second medium
$\tilde{\underline{l}}_3$, $\underline{l}_3$	vectors describing the path of the light through the third medium

Position Vectors

$\underline{X}_F$	locates the origin with respect to the characteristic focal point of the lens
$\tilde{\underline{X}}_A$, $\underline{X}_A$	locates where the beams strike the hydrocyclone wall relative to the origin
$\underline{X}_I$	vector describes position of the point of intersection of the beams relative to the origin
$\underline{e}_x$, $\underline{e}_y$, $\underline{e}_z$	unit base vectors describing coordinate system
$\underline{n}_A$	normal vector at hydrocyclone wall
$\underline{n}_B$	normal vector at wall of box

Other

$d_f(\underline{x})$	fringe spacing
f_d	doppler frequency
λ_i	wavelength of light in medium i
β_i	refractive index of medium i
$\langle u_i \rangle$	time-averaged velocity in i direction
ε	distance test section is moved
W	half-width of box

CHAPTER 1

INTRODUCTION

1.1 Motivation for this Study

Laser doppler anemometry (LDA) is a nonintrusive method of making local velocity measurements. A problem inherent in this technique is that refraction of the light beams occurs due to differences in the indices of refraction of the media through which the light beams traverse. The refraction phenomenon affects the focal length and angle of intersection of the light beams. The measuring point and velocity measurement are dependent upon these parameters.

LDA techniques take advantage of the frequency shift of the light to obtain velocity information about the flow field as follows (Durst et al., 1976):

$$\langle u_i \rangle(\underline{x}) = d_F(\underline{x}) \; \langle f_d(\underline{x}) \rangle \qquad (1.1)$$

where $\langle u_i \rangle(\underline{x})$ is the time-averaged velocity component of interest; $d_F(\underline{x})$ and $f_d(\underline{x})$ are the fringe spacing and doppler frequency, respectively.

When the flow is confined, the light beams refract due to the optical inhomogeneity of the various media. The refraction changes the focal length and half-angle of intersection of the light beams which are characteristic of the focusing lens. Thus, the actual measuring point, $\underline{x}$, and the fringe spacing, $d_F(\underline{x})$, change. d_F depends on the angle of the refracted beams and the wavelength, λ, of the light in the test medium. The relationship is (Durst, 1982)

$$d_F(\underline{x}) = \frac{\lambda}{2 \sin \theta_I(\underline{x})} \quad . \qquad (1.2)$$

The position vector $\underline{x}$ and the half-angle $\theta_I(\underline{x})$ of intersection of the light beams are dependent on the geometry of the test section, the optical properties of the media involved, and the position of the optics relative to the test section.

The test section under investigation is a hydrocyclone (see Figure 1.1). Although the hydrocyclone is a centrifugal separator commonly used, the flow field within the device is not well understood. Previously, the flow patterns in the hydrocyclone were investigated by means of flow visualization techniques (Dabir, 1983; Knowles, 1971; Bradley and Pulling, 1959; Kelsall, 1952). The advent of laser doppler anemometry provides a much more precise method and allows for a much more detailed study of flow fields. Unfortunately, the geometry of the hydrocyclone does not lend itself to a direct application of the method. Refraction of the light beams occurs due to the curvature of the hydrocyclone and the optical inhomogeneity of the various media.

1.2 A Review of Other Strategies in the Literature

The corrections presented in the literature are developed with the incident beams either in a plane perpendicular or coaxial with the axis of symmetry of the hydrocyclone (depending on whether tangential or axial velocity measurements are made). This is done to assure that the two beams will intersect. If the beams are oriented differently, the curvature of the vessel wall makes it difficult to position the beams at the desired point of measurement such that they intersect and allow the proper velocity vector to be measured.

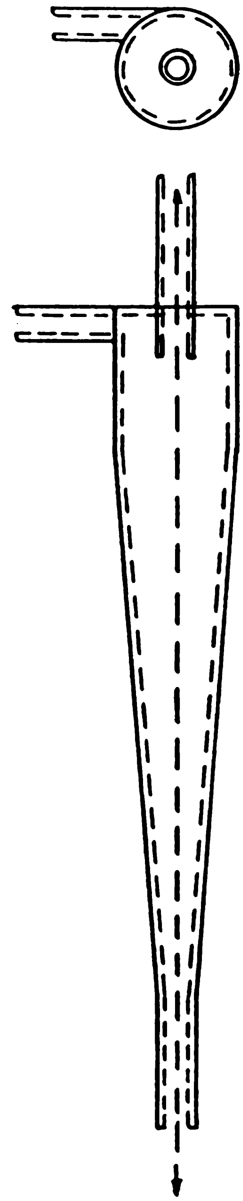

Figure 1.1 . Hydrocyclone.

Boadway and Karahan (1981) developed corrections for axial and tangential velocity measurements in cylindrical geometries (with the beams oriented in the aforementioned manner). Corrections for the refraction at both surfaces of the vessel wall were made. Small-angle linearizations were used in the development of their corrections. The error incurred by doing this is unknown.

Durst et al. (1981) suggest that the test fluid be selected to match the index of refraction of the vessel confining the flow. This eliminates the refraction at the inner wall of the vessel. This may not always be done however if particular fluid properties are desired.

TSI (1980) suggests building a box around the test vessel with a material of the same index of refraction of the vessel. The space between the vessel and the box is then filled with a fluid that matches the refractive index of the chamber walls (box and vessel). This method eliminates the need to correct for the refraction due to the curvature of the outer vessel wall while allowing a free selection of test fluid. Cross sections of the test section are shown in Figure 1.2. Durst (1976) and TSI (1980) present methods of correcting for the refraction of a light beam passing through three plane parallel layers of different refractive indices using geometric optics. These methods are also valid for correcting axial velocity measurements in test sections which include cylindrical geometries if the plane containing the incident beams also contains the vertical axis of symmetry of the cylinder. These corrections were developed using a small-angle approximation (i.e., $\theta << 15^{o}$). Corrections for velocity measurements in conical test sections were not developed.

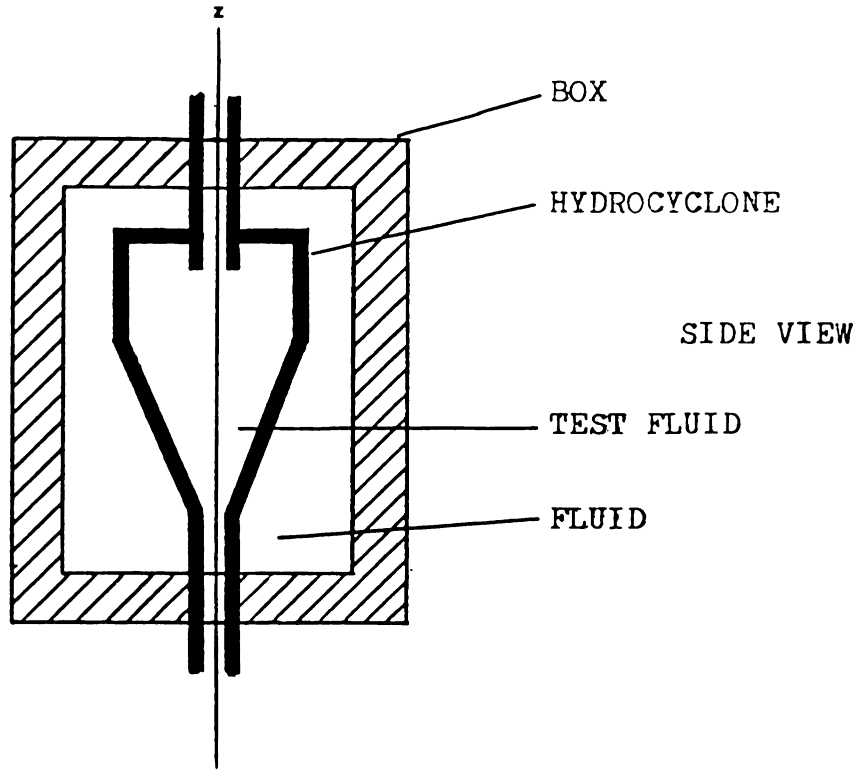

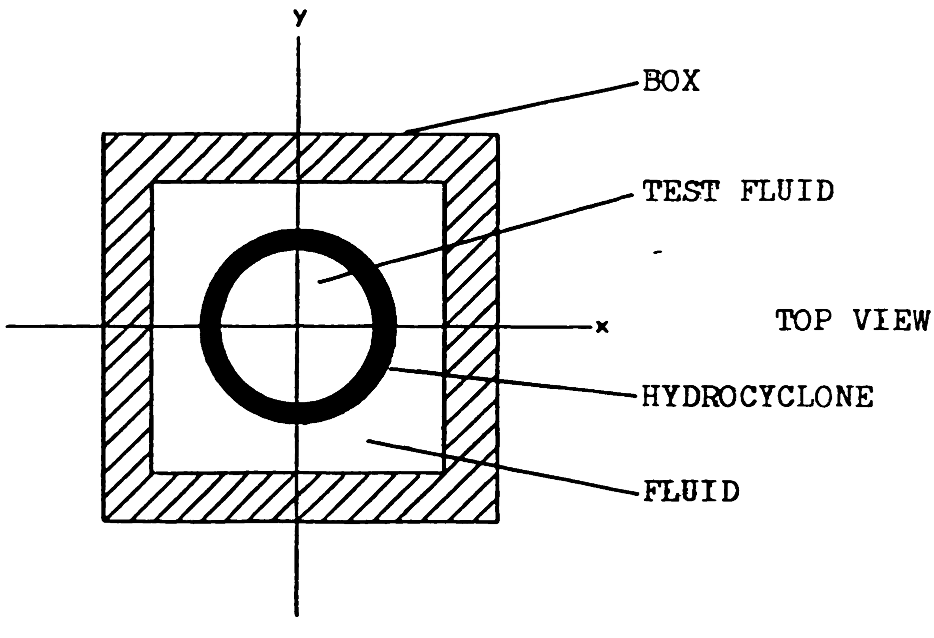

Figure 1.2 . Cross-sections of the test section.

Dabir (1983), also developed corrections for the test section shown in Figure 1.2. Correction were developed for axial and tangential velocity measurements in both the conical and cylindrical sections. For test sections which include these geometries, however, the corrections are again dependent upon the plane of the incident beams with respect to the axis of symmetry of the test section. Small-angle approximations were used in the development of the corrections. The range of system parameters over which the small-angle approximations are valid remains unexplored.

1.3 Objectives of this Research

The primary objective of this work is to develop the corrections required due to the refraction phenomena when laser doppler anemometry is used to make velocity measurements in test sections of cylindrical and conical geometries (see Figure 1.2). The corrections are necessary if accurate quantitative information is to be obtained about the flow using laser doppler techniques.

Many researchers report uncorrected laser doppler velocity measurements and one of the goals of this study is to determine the measurement error due to the neglect of this phenomenon. This is particularly important if the radial velocity profiles are to be calculated using the measured axial velocity profiles (Dabir, 1983).

Because the movement of the beams does not directly correspond to the movement of the laser or test section (depending upon how the profiles are made) the sensitivity with which the measurements may be made with respect to the design of the test section and choice of building materials and fluids will be examined. This will provide insight into the design of a test section which allows measurements to be made on a finer scale.

1.4 Basic Principles

1.4.1 Laser Doppler Anemometry

The ability to use LDA as a method of obtaining velocities stems from light scattering theory (Born and Wolf, 1959; Mie, 1908). The generation of laser doppler signals in a dual-beam differential doppler system results from particles scattering light while moving through a region in space common to both incident light beams. This region is referred to as the measuring or probe volume of the LDA system.

Figure 1.3 shows the components of a typical LDA dual-beam system. As shown in the figure, the light collection arrangement is in the forward scattering mode. The performance of the forward and backscattering light collection arrangements is compared by Cheung and Koseff (1982).

The paths of the beams relative to the velocity component of interest are presented in Figure 1.4. The velocity vector lies in the optical plane of the incident beams and is perpendicular to the optical bisector. When two coherent light beams intersect, a fringe pattern results due to the interference of wave fronts (see Figure 1.5). The fringes may be detected using square-law detectors for electromagnetic waves which can resolve the fringes spatially and which have a much larger response time than the period of the light waves (Durst, 1970).

Two interpretations have been used to explain the generation of the doppler signal. Rudd (1969) showed that the signal received by the photodetector can be understood to result from particles crossing the interference fringes and scattering light (this interpretation is termed the "fringe model" in the literature). As the particle crosses the fringes it blocks off and scatters varying amounts of light. This

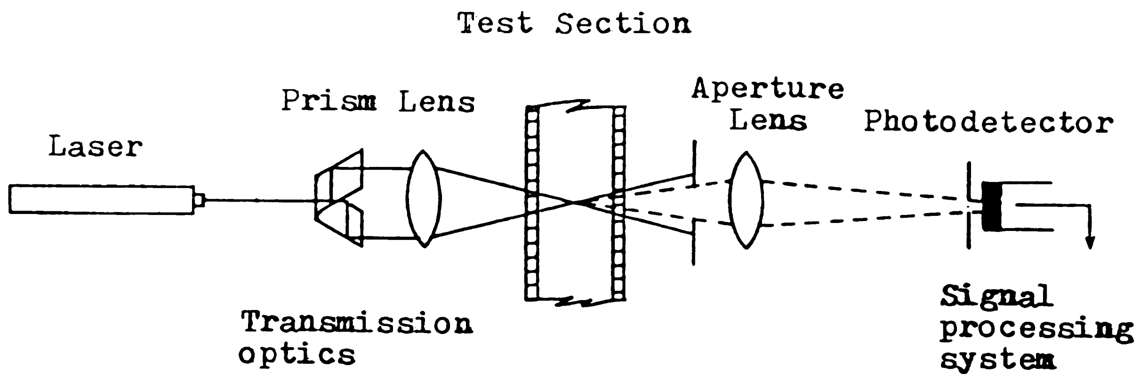

Figure 1.3 . Components of a dual beam differential doppler LDA system.

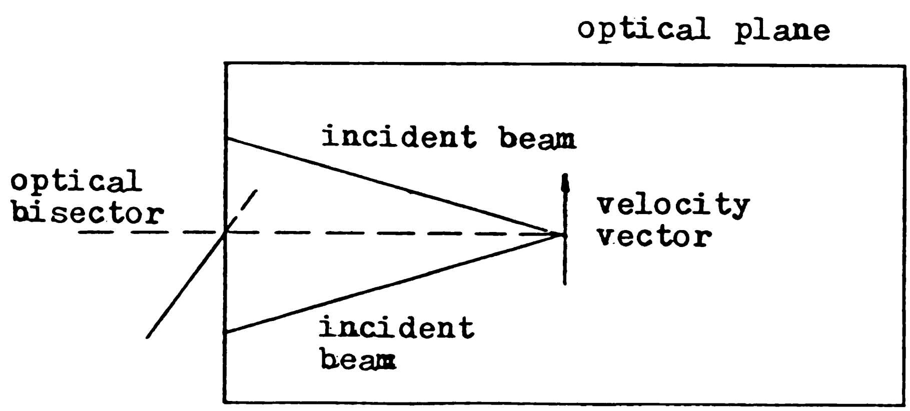

Figure 1.4 . Orientation of the beams relative to the velocity vector of interest.

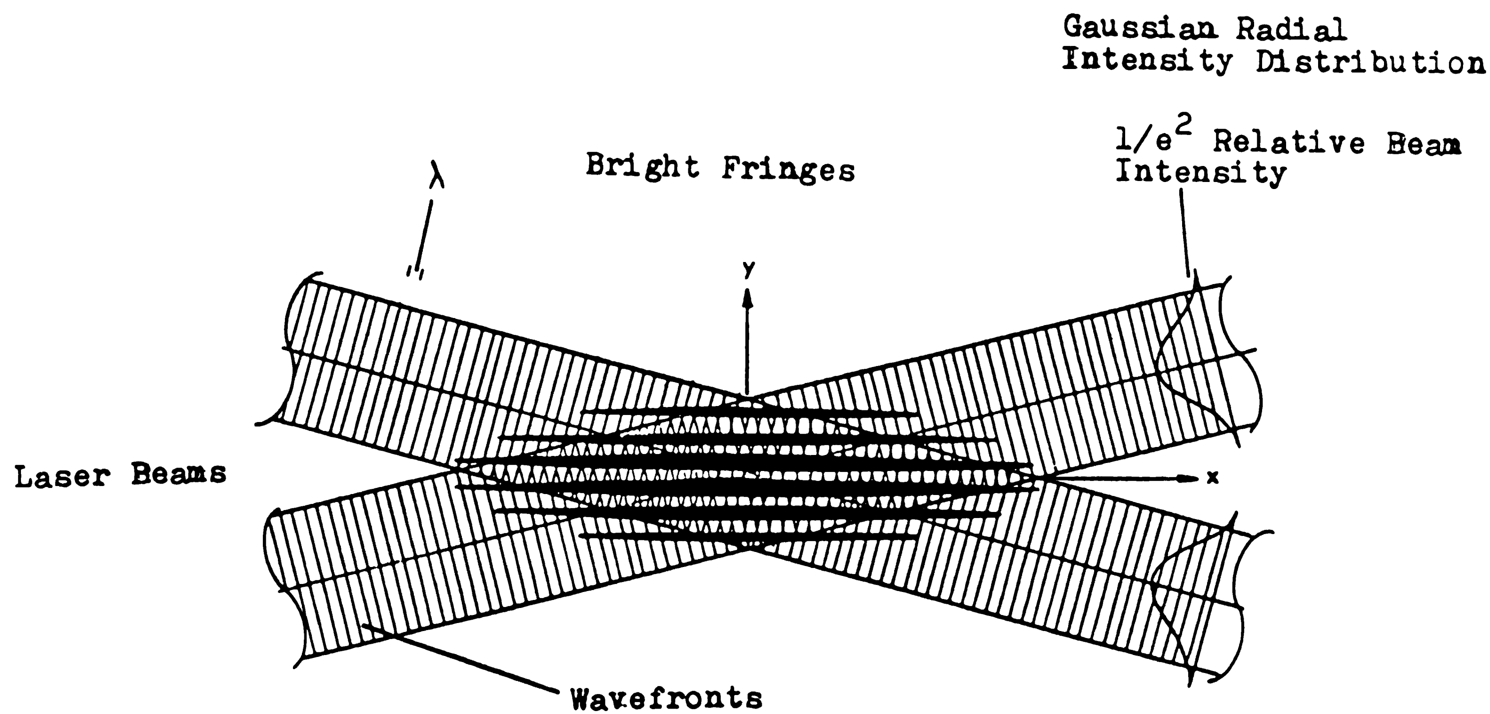

Figure 1.5 . Fringe pattern due to the intersection of two coherent laser beams.

variation in the intensity of the signal is used to determine the frequency shift of the light (DISA, Publ. no. 8208E).

Durst (1982) pointed out that for a particle to experience a fringe it must interact with it for a time longer than the inverse of the wave frequency, but this does not actually occur. Instead, the signal is due to the scattering action of the particle and the properties of the photodetector. However the analytical result which relates the velocity to the frequency shift is the same regardless of the physical interpretation.

1.4.2 Geometric Optics

In geometric optics, the wave nature of light is ignored and the path of light is represented by rays. This may be done as long as the apertures or obstacles in the path of the light are much larger than the wavelength of the light.

The law of rectilinear propagation and the laws of reflection and refraction form the foundation of geometric optics. The law of rectilinear propagation states that in a homogeneous medium light travels in straight-line paths. The laws of reflection and refraction are analytically expressed as follows:

reflection $$\Psi = \Psi'' \tag{1.3a}$$

$$[\underline{\ell}_1(\Psi) \wedge \underline{\ell}_{re}(\Psi'')] \cdot \underline{n} = 0 \tag{1.3b}$$

refraction $$\beta_1 \sin \Psi = \beta_2 \sin \Psi' \tag{1.4a}$$

$$[\underline{\ell}_1(\Psi) \wedge \underline{\ell}_2(\Psi')] \cdot \underline{n} = 0 \quad . \tag{1.4b}$$

Ψ, Ψ', and Ψ'' are, respectively, the angles of the incident, refracted, and reflected beams relative to a unit normal vector $\underline{n}$ (see Figure 1.6). $\underline{\ell}_1$, $\underline{\ell}_2$, and $\underline{\ell}_{re}$ are vectors describing the paths of the incident, refracted, and reflected beams. The refractive index (β) of a medium is defined as the ratio of the speed of light in a vacuum to the speed in the medium.

Equations (1.3b) and (1.4b) state that the reflected and refracted rays lie in the plane formed by the incident ray and the normal to the surface at the point of incidence. Equations (1.3a) and (1.4a) define the angles of the reflected and refracted rays with respect to the normal to the surface, respectively. Derivations of the laws of geometric optics from electromagnetic theory are presented in Rossi (1957).

The change in wavelength as light travels from one medium to another may be determined using

$$\beta_i \lambda_i = \beta_j \lambda_j \qquad (1.5)$$

if the indices of refraction of the various media (β_1, β_2, β_3) and the wavelength of the incident light are known (Halliday and Resnick, 1974).

1.5 Illustration of the Refraction Phenomenon

Figures 1.7 and 1.8 show the paths of the beams through the test section when axial and tangential velocity measurements are made. Point I is the actual place where the two beams intersect. Point F is where the beams would intersect if all the media were optically homogeneous. Point O denotes the point of intersection of the optical bisector and the axis of symmetry of the hydrocyclone.

1.6 Methodology

Because it is desired to make all measurements relative to the center of the cyclone, point O is chosen as the origin of the coordinate system from which all positions ($\underline{X}_I$) will be described. The vector $\underline{X}_I$ describes

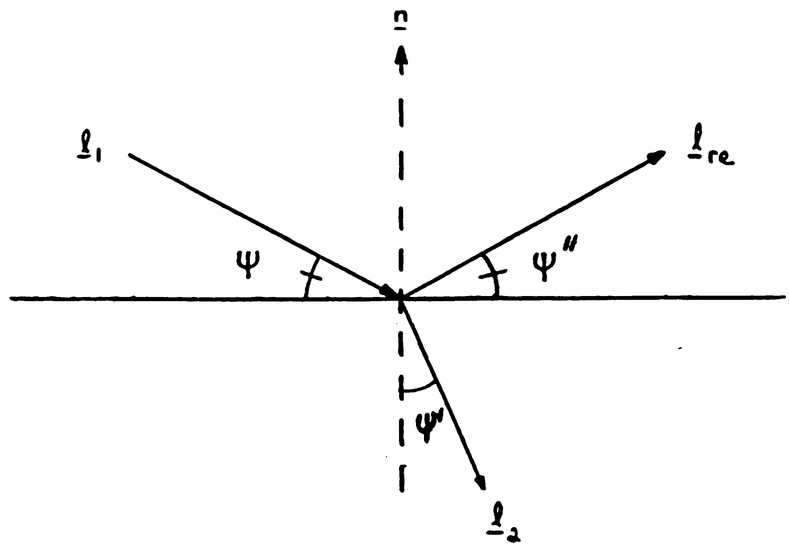

Figure 1.6 . Reflection and refraction of light at an interface.

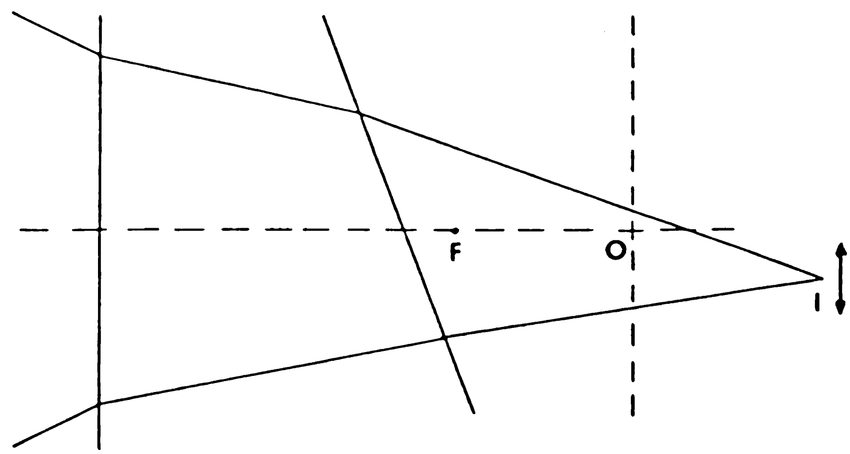

Figure 1.7 . Illustration of the refraction of the beams when axial measurements are made.

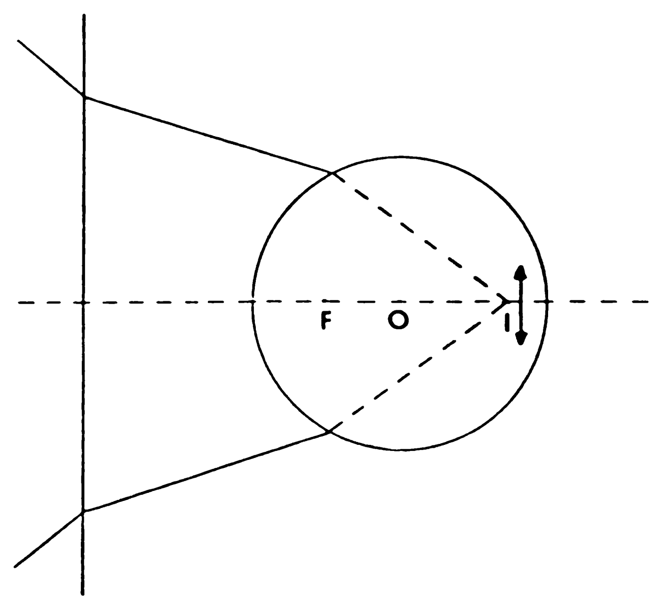

Figure 1.8 . Illustration of the refraction of the beams when tangential measurements are made.

where the light beams intersect relative to the origin (see Figures 1.9 and 1.10). The origin (point O) is not stationary in space however. In obtaining velocity profiles, measurements are made across the radius of the cyclone. To do this, the test section is moved. Thus, some stationary point of reference is needed from which to locate the origin. Point F is chosen because it is fixed in space, being only dependent on the radius of curvature of the focusing lens. An alternate choice for the stationary point of reference could have been the focusing lens. The difference between the two possible points of reference is the characteristic focal length of the lens. The vector $\underline{X}_F$ locates the origin relative to the fictitious focal point "F". Figure 1.11 shows the physical significance of $\underline{X}_F$ for each of the velocity measurements.

X_{FX}, defined as $\underline{X}_F \cdot \underline{e}_X$, is

$$X_{FX} = X^{O}{}_{FX} + \varepsilon \quad . \tag{1.6}$$

$X^{O}{}_{FX}$ is the distance from the origin to the lens focal point (point F) when the beams intersect at the origin; and, ε is the distance the test section is moved off center.

The problem now becomes one of determining $\underline{X}_I$ and $\theta_I(\underline{X})$. An analytical solution to the problem is presented in Chapter 2.

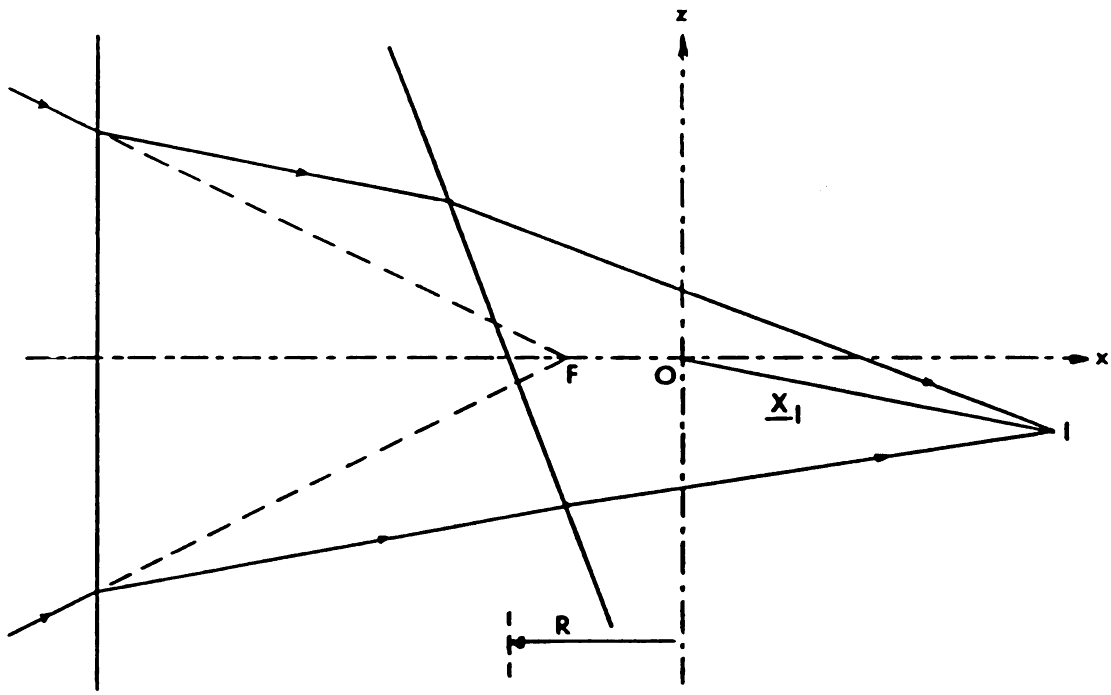

Figure 1.9 . The position vector for axial measurements.

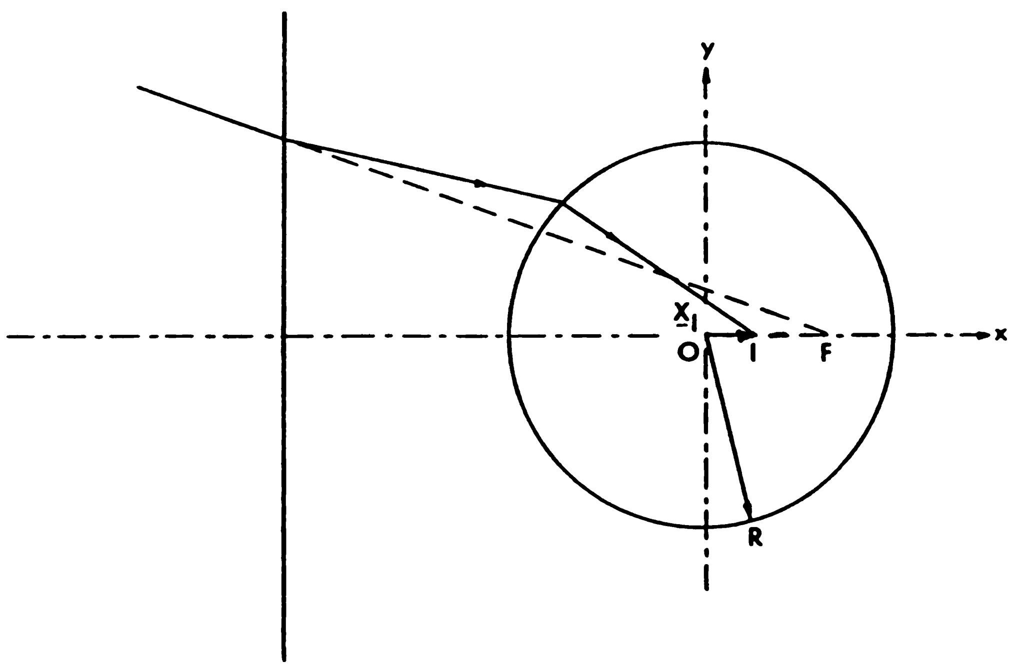

Figure 1.10 . The position vector for tangential measurements.

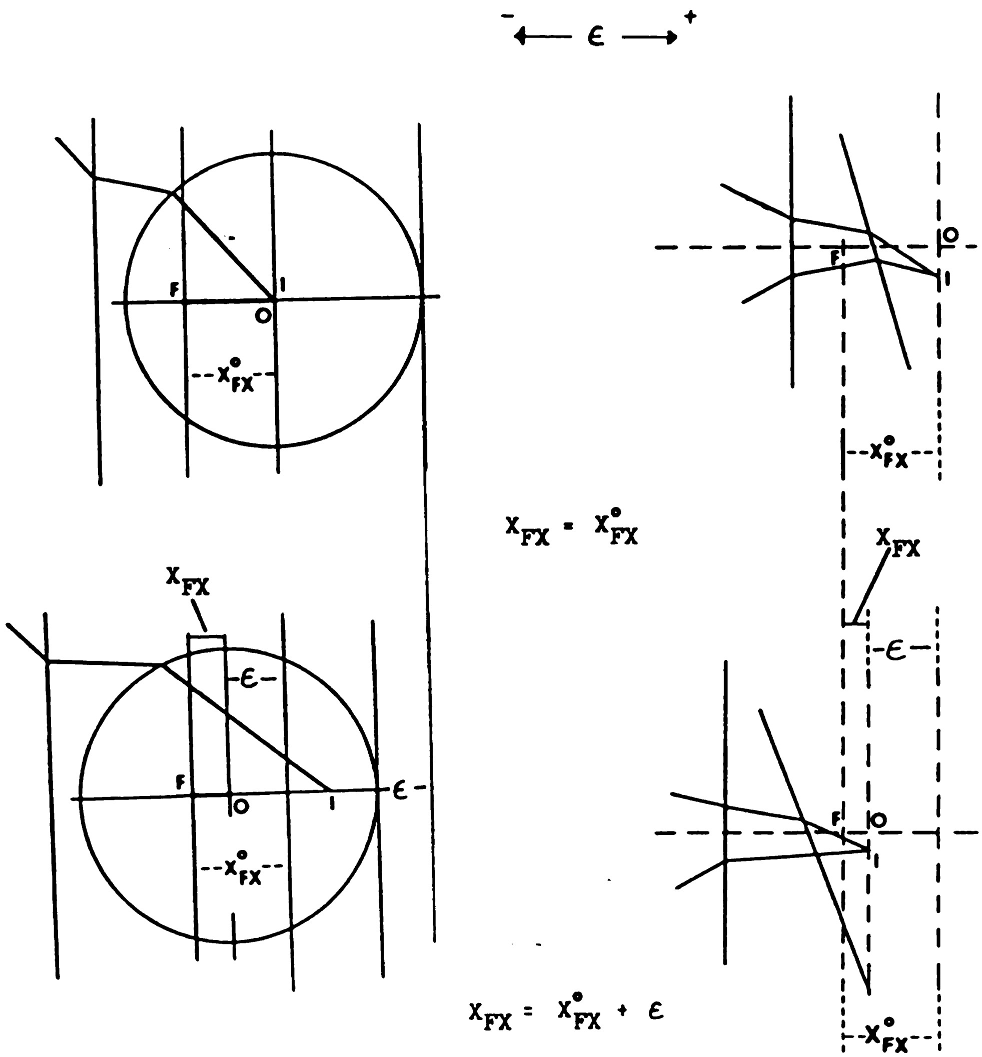

Figure 1.11 . Illustration of X_{FX} for each of the measurements.

CHAPTER 2

DEVELOPMENT OF THE REFRACTION CORRECTIONS

2.1 Coordinate System

Solution of the problem requires an analytical representation of the paths of the beams. A coordinate system (see Figure 2.1) is established such that the optical bisector ($\underline{OB}$) is colinear with the x-axis and the axis of symmetry of the hydrocyclone ($\underline{AS}$) is colinear with the z-axis.

$$\underline{AS} = \underline{e}_Z \tag{2.1a}$$

$$\underline{OB} = \underline{e}_X \tag{2.1b}$$

$$(\underline{AS} \wedge \underline{OB}) \cdot \underline{e}_Y = 1 \tag{2.1c}$$

An orthogonal rectilinear coordinate system is used because it corresponds to the directional (X,Y,Z) mobility of the test section. The test section may be moved from side-to-side and up-and-down with the use of a milling table and hydraulic jack as shown in Figure 2.2.

2.2 Normal Vectors

The normal vectors illustrated in Figure 2.3 can be written as

$$\underline{n}_B = -\underline{e}_X \tag{2.2}$$

$$\underline{n}_A = [-\cos\theta_A\underline{e}_X + \sin\theta_A\underline{e}_Y]\cos\theta_H - \sin\theta_H\underline{e}_Z \tag{2.3}$$

For axial velocity measurements, the plane of the incident laser beams is set up to include the axis of symmetry of the cyclone. θ_A is therefore zero. The normal vectors are then

$$\underline{n}_B = -\underline{e}_X \tag{2.4}$$

$$\underline{n}_A = -\cos\theta_H\underline{e}_X - \sin\theta_H\underline{e}_Z \quad . \tag{2.5}$$

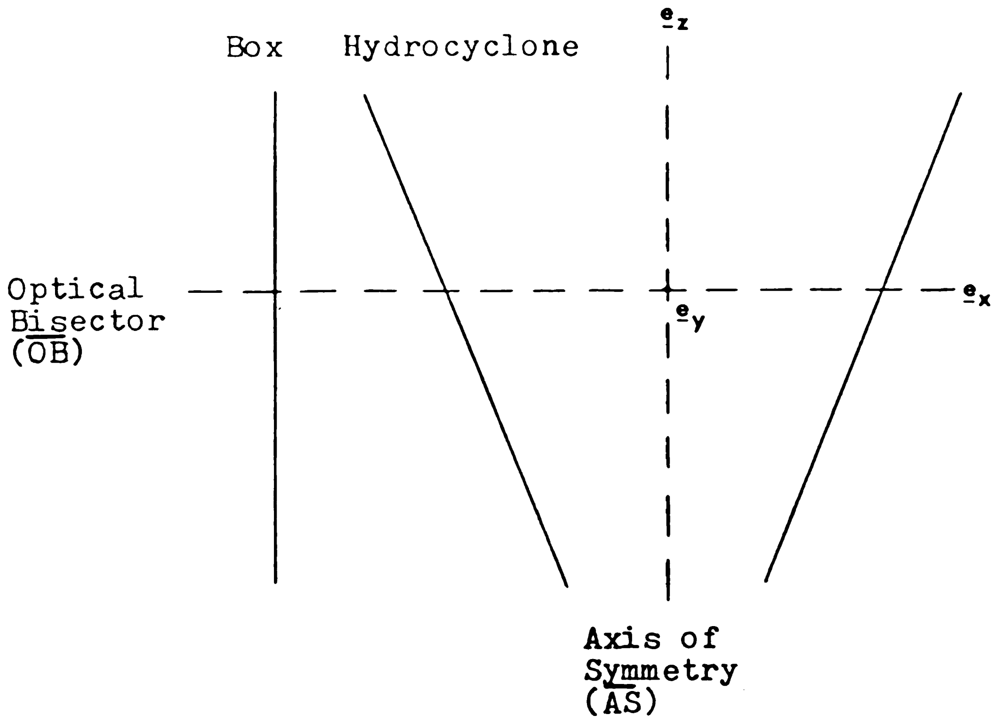

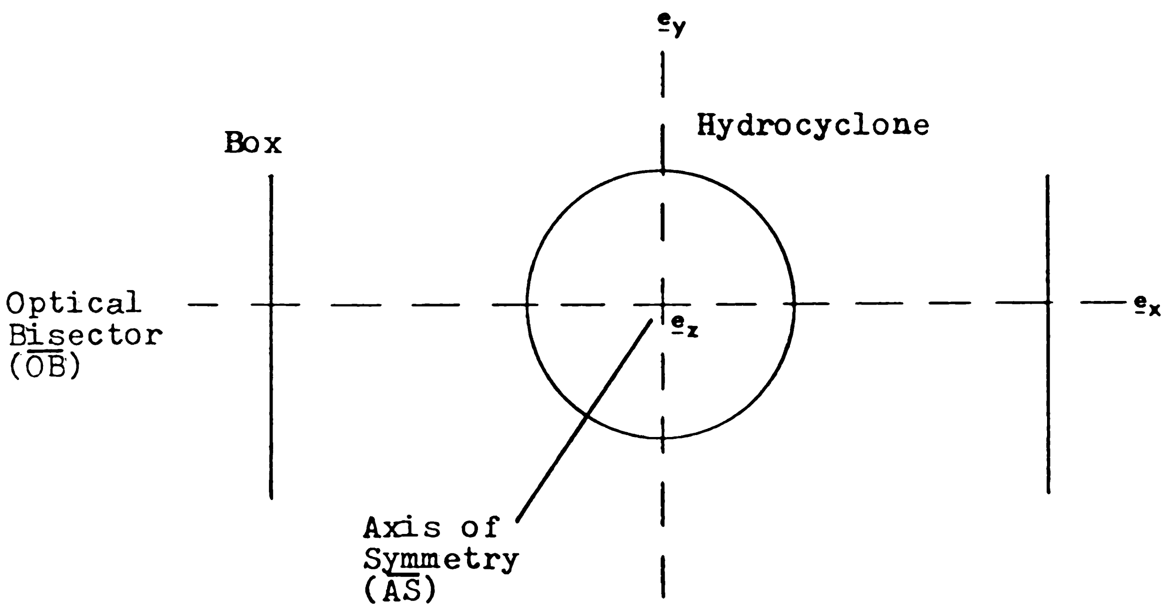

Figure 2.1 . The Coordinate System.
(e_x, e_y, and e_z are unit base vectors)

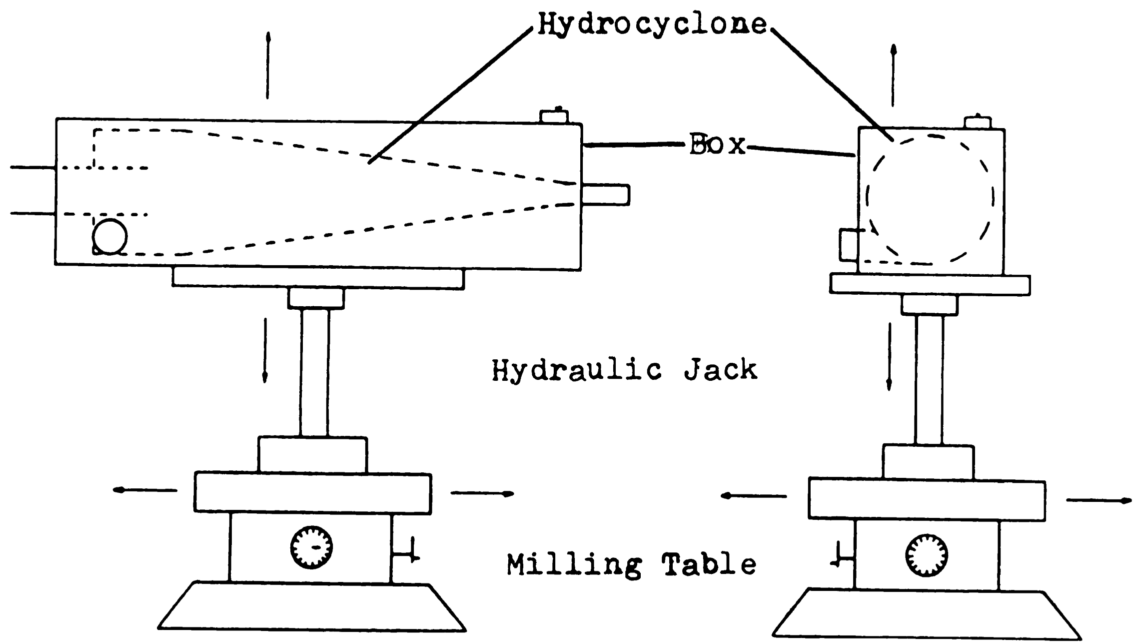

Figure 2.2 . Mobility of the test section.

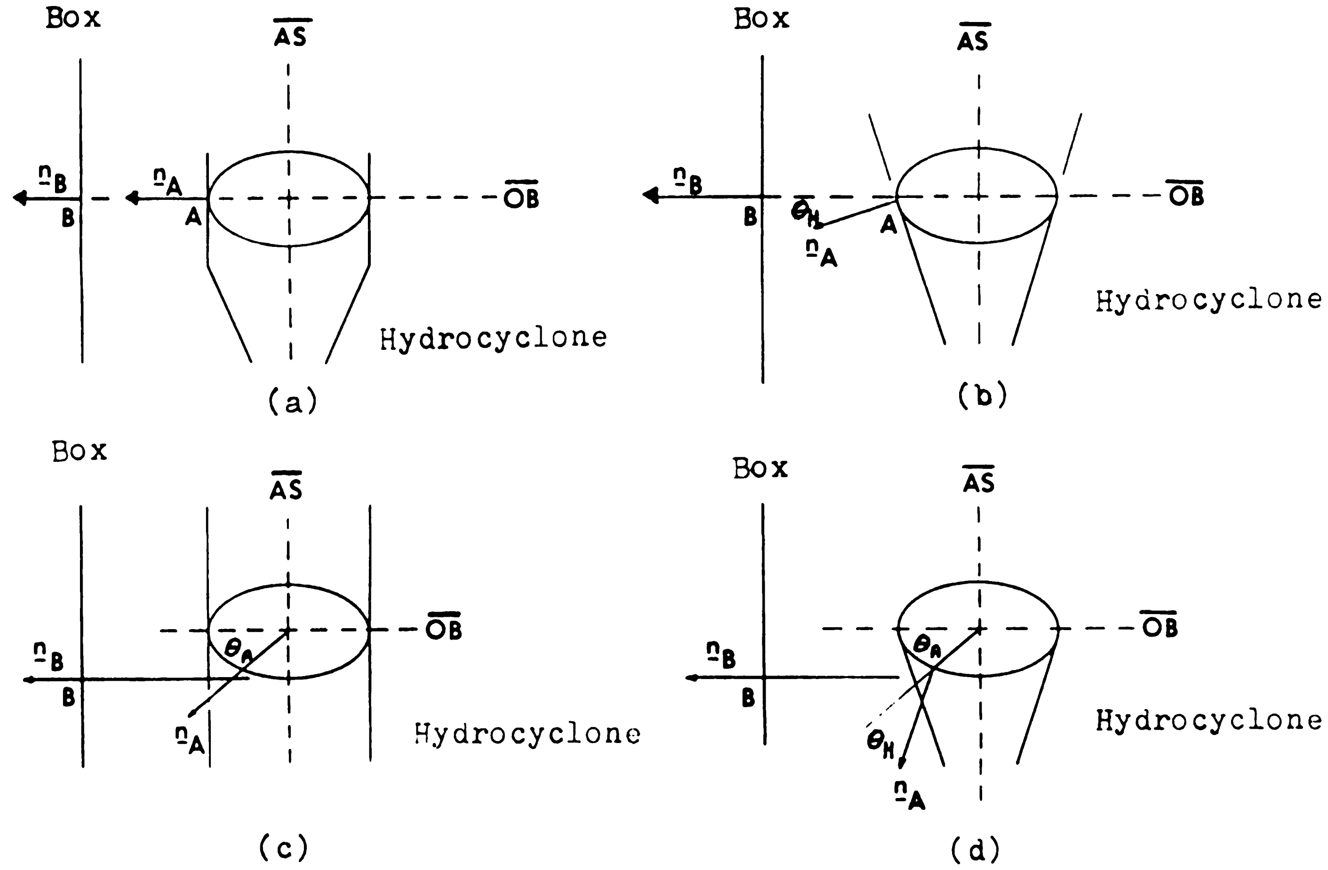

Figure 2.3 . The normal vectors: (a) Axial measurements in the cylindrical section, (b) Axial measurements in the conical section, (c) Tangential measurements in the cylindrical section, (d) Tangential measurements in the conical section.

For the cylindrical section, $\theta_H = 0$ and the normal vectors reduce to

$$\underline{n}_A = \underline{n}_B = -\underline{e}_X \quad . \tag{2.6}$$

For tangential velocity measurements, the plane of the incident beams is set up to be perpendicular to the axis of symmetry of the hydrocyclone. θ_A which defines where the beams intersect the wall of the cyclone with respect to the x-axis is nonzero for this case. Equations (2.2) and (2.3) represent the normal vectors for the conical section. For the cylindrical section, $\theta_H = 0$; therefore, Equation (2.3) simplifies to

$$\underline{n}_A = -\cos\theta_A \underline{e}_X + \sin\theta_A \underline{e}_Y \quad . \tag{2.7}$$

2.3 Analysis to obtain θ_I

The position of the incident beams with respect to the test section depends on whether axial or tangential velocity measurements are made (see Figure 2.4). For axial measurements, the equations describing the incident beams ($\underline{l}_1$ and $\tilde{\underline{l}}_1$) are:

$$\underline{l}_1 \cdot \underline{l}_1 = 1 \tag{2.8}$$

$$\underline{l}_1 \cdot \underline{e}_Y = 0 \tag{2.9}$$

$$-\underline{l}_1 \cdot \underline{n} = \cos k \tag{2.10}$$

$$\underline{l}_1 = \underline{\underline{Q}} \cdot \tilde{\underline{l}}_1 \quad . \tag{2.11}$$

For tangential measurements, Equation (2.9) is replaced with

$$\underline{l}_1 \cdot \underline{e}_Z = 0 \quad . \tag{2.9a}$$

The incident beans $\underline{l}_1$ and $\tilde{\underline{l}}_1$ are related through a reflection matrix $\underline{\underline{Q}}$ which is defined as follows

$$\underline{\underline{Q}} = \begin{bmatrix} 1 & 0 & 0 \\ 0 & -1 & 0 \\ 0 & 0 & -1 \end{bmatrix} \quad . \tag{2.12}$$

The equations that describe the path of a beam through the second medium (see Figure 2.5) are:

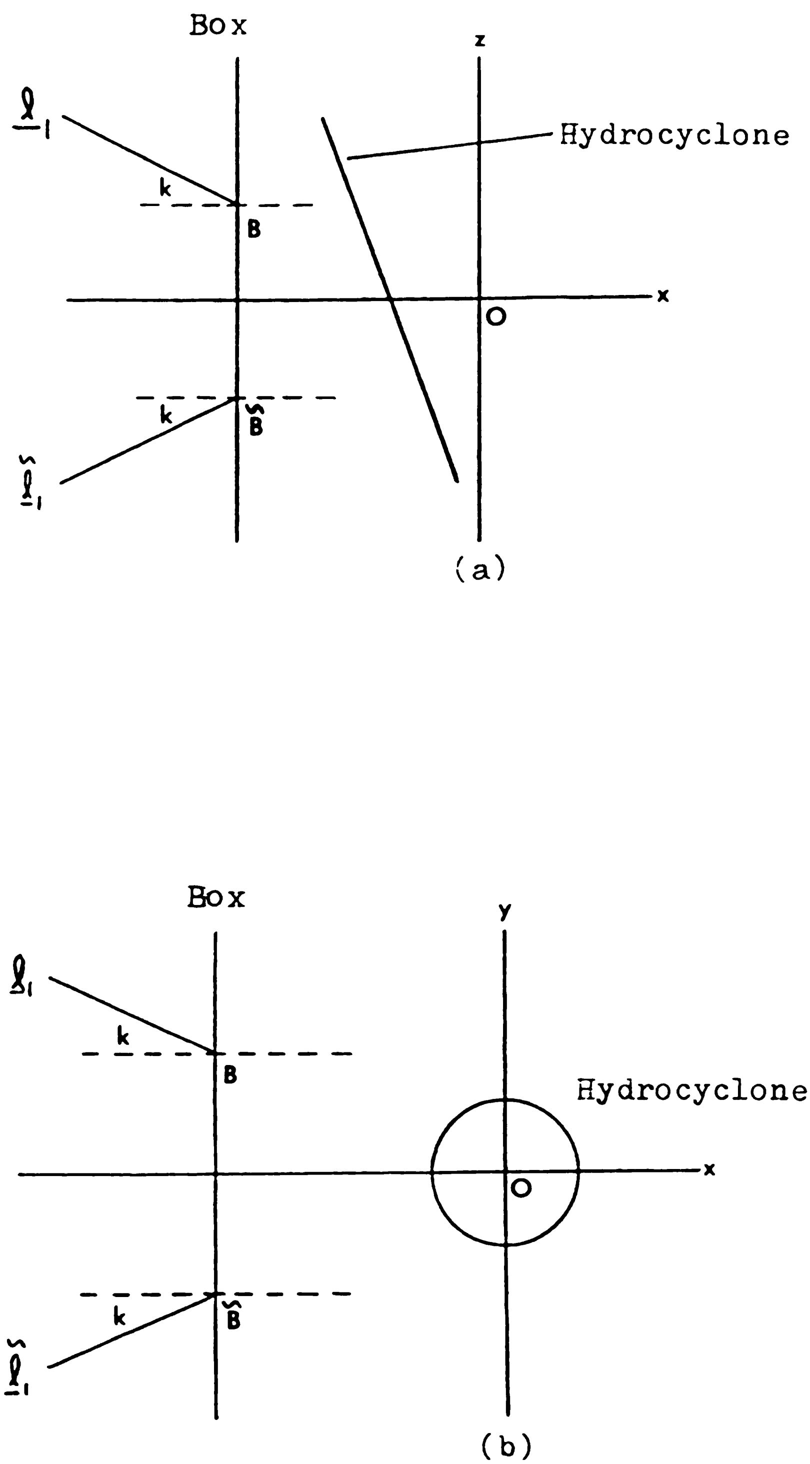

Figure 2.4 .. Orientation of the beams with respect to the test section : (a) axial measurements; (b) tangential measurements.

$$\beta_1 \sin k = \beta_2 \sin \theta_{2B} \quad (2.13)$$

$$(\underline{l}_1 \wedge \underline{l}_2) \cdot \underline{n}_B = 0 \quad (2.14)$$

$$\underline{l}_2 \cdot \underline{l}_2 = 1 \quad (2.15)$$

$$-\underline{l}_2 \cdot \underline{n}_B = \cos\theta_{2B} \quad . \quad (2.16)$$

Equation (2.13) defines the angle of the refracted beam relative to the normal of the first interface. Equations (2.14)-(2.16) define the three components of the vector $\underline{l}_2$.

The paths of the beams through the second medium remain reflections of each other when considered with respect to the first interface using the angle θ_{2B} as defined above, the $\tilde{\underline{l}}_2$ may be found using

$$\underline{l}_2 = \underline{\underline{Q}} \cdot \tilde{\underline{l}}_2 \quad . \quad (2.17)$$

The refracted beams are then described relative to the second interface as follows:

$$-\underline{l}_2 \cdot \underline{n}_A = \cos\theta_{2A} \quad (2.18)$$

$$-\tilde{\underline{l}}_2 \cdot \tilde{\underline{n}}_A = \cos\tilde{\theta}_{2A} \quad . \quad (2.19)$$

These equations provide the angles (see Figure 2.6) that describe the beams relative to the normal of the second interface. The following equations describe the paths of the beams through the third medium:

$$\beta_2 \sin\theta_{2A} = \beta_3 \sin \theta_{3A} \quad (2.20)$$

$$-\underline{l}_3 \cdot \underline{n}_A = \cos \theta_{3A} \quad (2.21)$$

$$\underline{l}_3 \cdot \underline{l}_3 = 1 \quad (2.22)$$

$$(\underline{l}_2 \wedge \underline{l}_3) \cdot \underline{n}_A = 0 \quad (2.23)$$

and

$$\beta_2 \sin\tilde{\theta}_{2A} = \beta_3 \sin \tilde{\theta}_{3A} \quad (2.24)$$

$$-\tilde{\underline{l}}_3 \cdot \tilde{\underline{n}}_A = \cos \tilde{\theta}_{3A} \quad (2.25)$$

$$\tilde{\underline{l}}_3 \cdot \tilde{\underline{l}}_3 = 1 \quad (2.26)$$

$$(\tilde{\underline{l}}_2 \wedge \tilde{\underline{l}}_3) \cdot \tilde{\underline{n}}_A = 0 \quad . \quad (2.27)$$

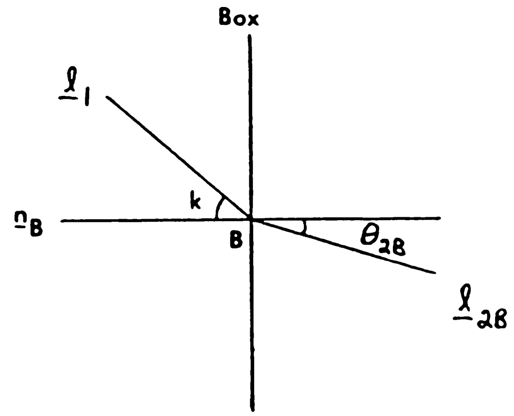

Figure 2.5 . Refraction across the first interface.

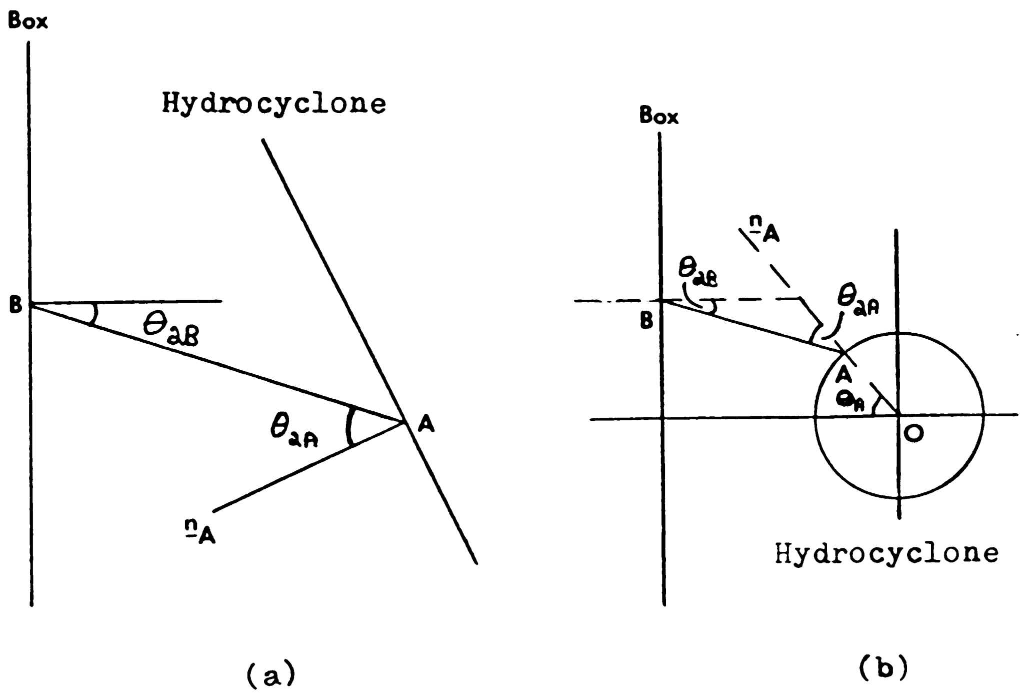

Figure 2.6 . Relation of ℓ_a to the interfaces: (a) axial measurements; (b) tangential measurements.

Because the vectors $\underline{l}_2$, $\underline{l}_3$, and $\underline{n}_A$ are all in the same plane, the vector $\underline{l}_3$ can be written

$$\underline{l}_3 = a\underline{l}_2 + b\underline{n}_A \quad . \tag{2.28}$$

This equation may be used in place of one of the Equations (2.20) - (2.23). $\tilde{\underline{l}}_3$ may be determined similarly. Once $\underline{l}_3$ and $\tilde{\underline{l}}_3$ are known, the half-angle of intersection of the laser beams in the test section (see Figure 2.7) may be obtained from

$$\underline{l}_3 \cdot \tilde{\underline{l}}_3 = \cos(2\theta_I) \quad . \tag{2.29}$$

2.4 Analysis to obtain $\underline{X}_I$

The position vector (see Figure 2.8) may be written

$$\underline{X}_I = \underline{X}_A + \overline{AI}\,\underline{l}_3 \quad . \tag{2.30}$$

Because of the way the optics and test section are aligned with respect to the coordinate system, there is no y-component in the vector describing the point of intersection of the light beams.

$$\underline{X}_I \cdot \underline{e}_Y = 0 \tag{2.31}$$

The other components of $\underline{X}_I$ are found from

$$X_{IX} = \underline{X}_I \cdot \underline{e}_X = \underline{X}_A \cdot \underline{e}_X + \overline{AI}\underline{\ell}_3 \cdot \underline{e}_X \tag{2.32}$$

and

$$X_{IZ} = \underline{X}_I \cdot \underline{e}_Z = \underline{X}_A \cdot \underline{e}_Z + \overline{AI}\underline{\ell}_3 \cdot \underline{e}_Z \tag{2.33}$$

The vector $\underline{X}_A$ and the angle θ_A (which is required in defining $\underline{n}_A$ for the tangential measurements) are as yet undetermined. These unknowns are obtained from a geometric analysis of the system.

2.4.1 Axial Measurements

When the beams are positioned for axial measurements, $\underline{X}_A$ (see Figure 2.9) is defined by

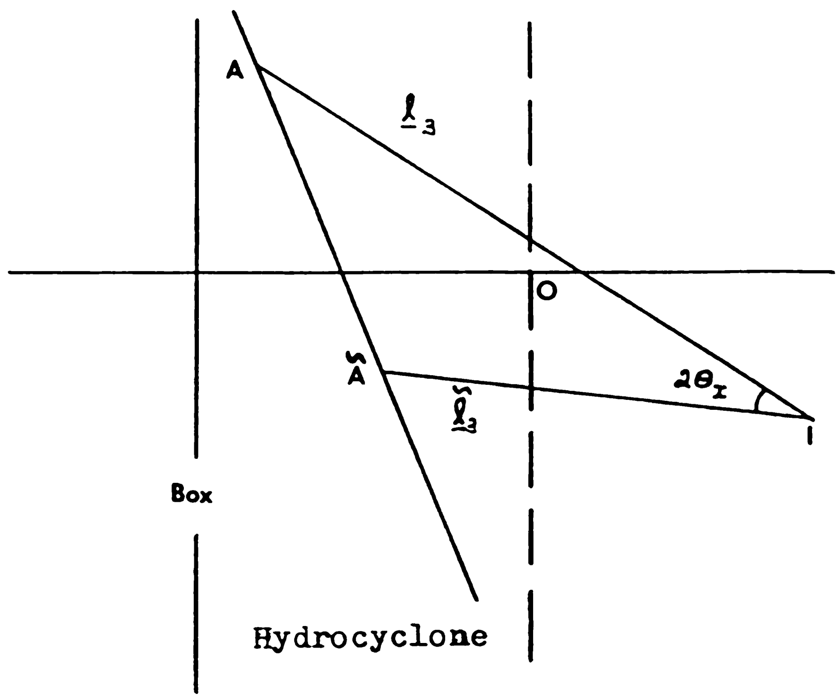

(a)

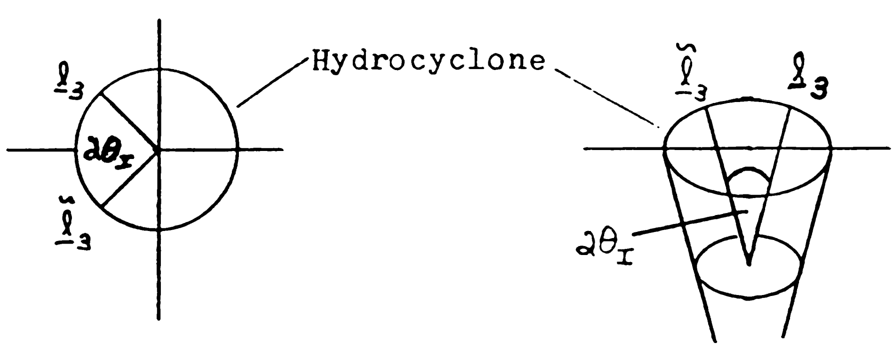

(b)

Figure 2.7 . The half-angle θ_I : (a) axial measurements; (b) tangential measurements.

$$\underline{X}_A = -R\,\underline{e}_X + \overline{DA}\,\underline{1}_H \tag{2.34}$$

and

$$\underline{X}_A = \underline{X}_B + \overline{BA}\,\underline{1}_2 \tag{2.35}$$

where

$$\underline{1}_H = -\sin\theta_H\underline{e}_X + \cos\theta_H\underline{e}_Z \tag{2.36}$$

$$\underline{X}_B = -W\underline{e}_X + \overline{CB}\,\underline{e}_Z \tag{2.37}$$

and

$$\overline{CB} = (W + X_{FX})\tan k \quad . \tag{2.38}$$

Equating the two expressions for $\underline{X}_A$ results in the following component equations:

$$\underline{e}_X:\quad -R - \overline{DA}\sin\theta_H = -W + \overline{BA}\cos\theta_{2B} \tag{2.39}$$

$$\underline{e}_Z:\quad \overline{DA}\cos\theta_H = (W + X_{FX})\tan k - \overline{BA}\sin\theta_{2B} \tag{2.40}$$

Manipulating these equations results in the following equation for $\overline{DA}$.

$$\overline{DA} = \frac{(W+X_{FX})\tan k - (W-R)\tan\theta_{2B}}{\cos\theta_H - \sin\theta_H\tan\theta_{2B}} \tag{2.41}$$

Equation (2.34) may then be written as follows:

$$\underline{X}_A = -R\underline{e}_X + \left[\frac{(W+X_{FX})\tan k - (W-R)\tan\theta_{AB}}{\cos\theta_H - \sin\theta_H\tan\theta_{2B}}\right]\left[-\sin\theta_H\underline{e}_X + \cos\theta_H\underline{e}_Z\right] \quad . \tag{2.42}$$

The position vector is also defined by

$$\underline{X}_I = \underline{\tilde{X}}_A + \tilde{A}\tilde{I}\,\underline{\tilde{\ell}}_3 \tag{2.43}$$

where $\underline{\tilde{X}}_A$ may be determined in the same manner as $\underline{X}_A$. Similarly, $\overline{AI}$ may be found by equating the two equations for $\underline{X}_I$, Equations (2.30) and (2.43). The equation for $\overline{AI}$ is

$$\overline{AI} = \frac{M[\cos\theta_H + \sin\theta_H\tan(\theta_H - \tilde{\theta}_{3A})}{\sin(\theta_{3A} - \theta_H)\left[1 + \dfrac{\tan(\theta_H - \tilde{\theta}_{3A})}{\tan(\theta_{3A} - \theta_H)}\right]} \tag{2.44}$$

where

$$M = \left[\frac{(W+X_{FX})\tan k - (W-R)\tan\theta_{2B}}{\cos\theta_H - \sin\theta_H\tan\theta_{2B}} + \frac{(W+X_{FX})\tan k - (W-R)\tan\theta_{2B}}{\cos\theta_H + \sin\theta_H\tan\theta_{2B}}\right] \quad .$$

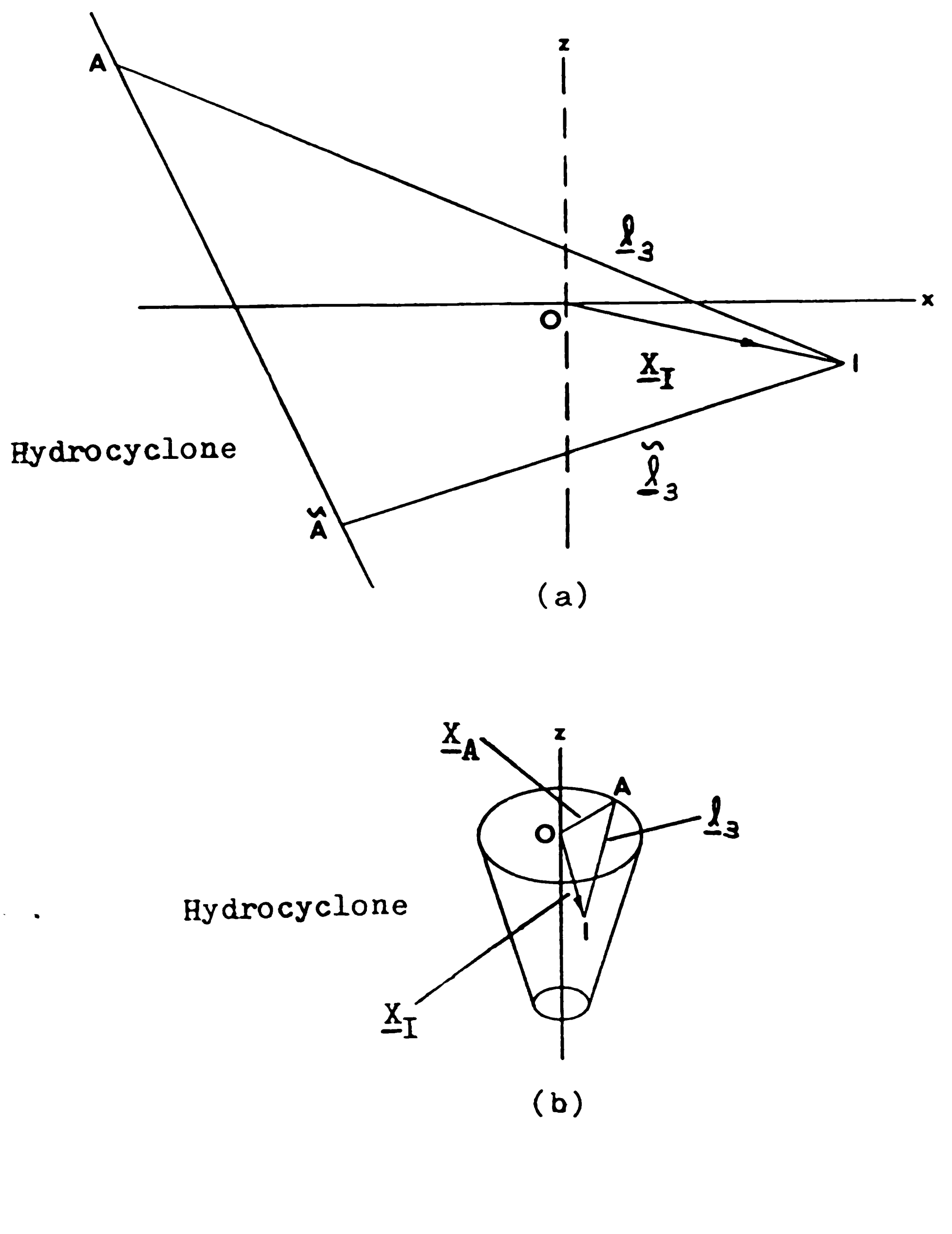

Figure 2.8 . The position vector $\underline{X}_I$: (a) axial measurements; (b) tangential measurements.

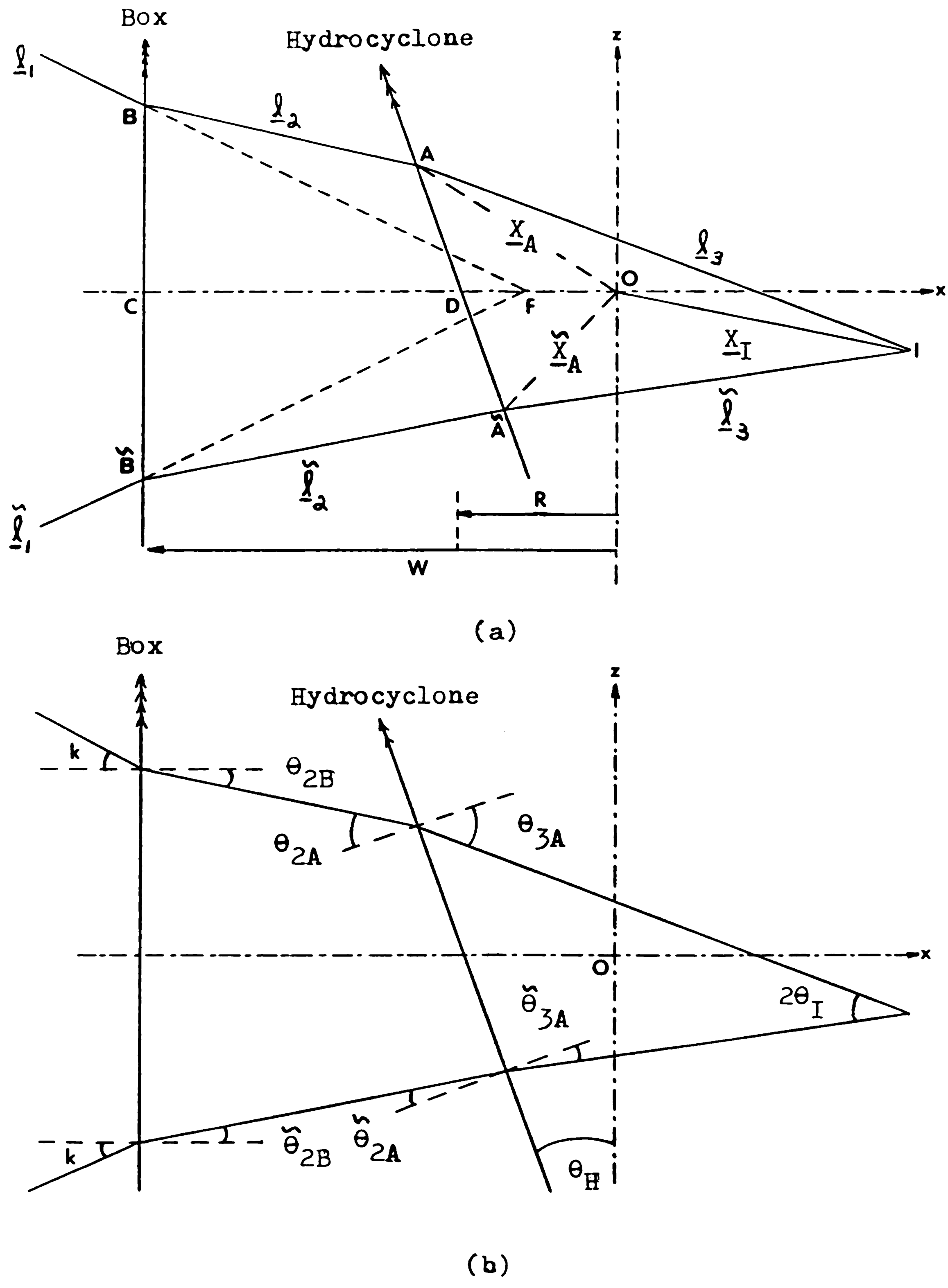

Figure 2.9 . Refraction of laser beams during axial velocity measurements : (a) vectors; (b) angles.

Equations (2.32) and (2.33) may then be used to obtain X_{IX} and X_{IZ}.

Using Equation (1.6) for X_{FX}, and noting that when ε equals zero, $X_{FX} = X^{o}_{FX}$. Therefore, X^{o}_{FX} can be calculated from Equation (2.32) with the result that

$$X^{o}_{FX} = -W + \frac{R(\cos^2\theta_H - \sin^2\theta_H \tan^2\theta_{2B}) + [(W-R)\tan\theta_{2B}] \left\{ \left[\frac{\cos\theta_H + \sin\theta_H \tan(\theta_H - \tilde{\theta}_{3A})}{\tan(\theta_{3A}-\theta_H) + \tan(\theta_H - \tilde{\theta}_{3A})}\right] 2\cos\theta_H - (\cos\theta_H + \sin\theta_H \tan\theta_{2B})\sin\theta_H \right\}}{\left[\frac{\cos\theta_H + \sin\theta_H \tan(\theta_H - \tilde{\theta}_{3A})}{\tan(\theta_{3A}-\theta_H) + \tan(\theta_H - \tilde{\theta}_{3A})}\right] 2\cos\theta_H \tan k - (\cos\theta_H + \sin\theta_H \tan\theta_{2B})\sin\theta_H \tan k} . \tag{2.45}$$

2.4.2 Tangential Measurements

For tangential measurements (see Figure 2.10), $\underline{X}_A$ is defined by the following equations:

$$\underline{X}_A = -R\cos\theta_A\,\underline{e}_X + R\sin\theta_A\,\underline{e}_Y \tag{2.46}$$

$$\underline{X}_A = -W\underline{e}_X + \overline{CB}\,\underline{e}_Y + \overline{BA}\,\underline{\ell}_2 \tag{2.47}$$

Once again, using Equation (1.6) for X_{FX}, and noting that $\theta_A = \theta_{2B}$, when $\varepsilon = 0$ yields the following equation for θ_A in terms of ε:

$$\sin\theta_A - \cos\theta_A \tan\theta_{2B} = \frac{\varepsilon \tan k}{R} \tag{2.48}$$

From Equation (2.31), $\overline{AI}$ can be described in terms of the other quantities as follows:

$$\overline{AI} = -\frac{\underline{X}_A \cdot \underline{e}_Y}{\underline{l}_3 \cdot \underline{e}_Y} \tag{2.49}$$

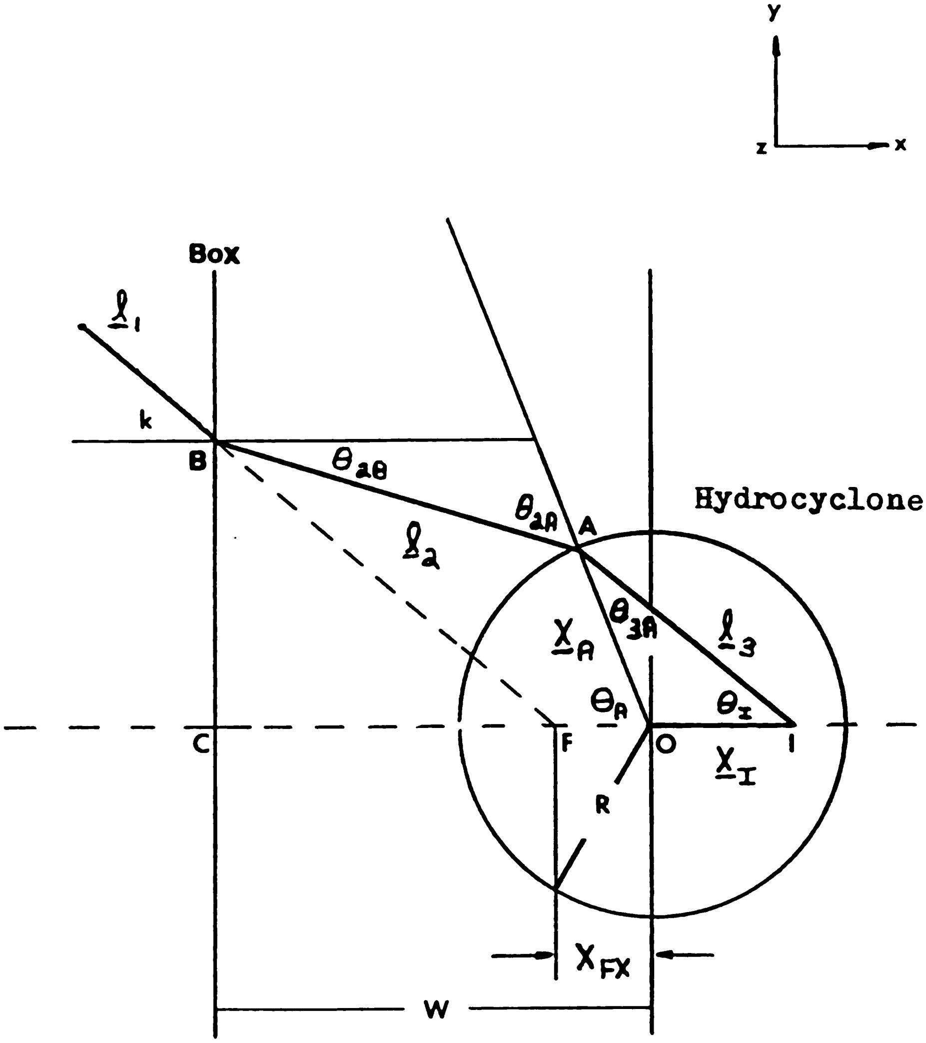

Figure 2.10 . Refraction of laser beam during tangential velocity measurements.

The preceeding development encompasses all the basic equations that are required in the solution of the problem. The working equations that result from the analysis and which are used in the development of the computer solution to the problem are presented in the following chapter.

CHAPTER 3

DISCUSSION

3.1 Corrections for Axial Measurements

The working equations used to develop the corrections for axial measurements are presented in Table 3.1. For axial measurements, there is a linear relationship between the movement of the test section and the movement of the beams. This can be seen from Equations (A) and (C) in Table 3.1. Also, the half-angle of intersection θ_I (and therefore the fringe spacing) is independent of the movement of the test section and the position where the measurement is made. This result was presented by Dabir (1983) for cylindrical geometries. From Equation (D) it can be seen that it is also true for conical geometries.

3.2 Corrections for Tangential Measurements

The corrections for tangential measurements are presented in Table 3.2. The position vector and the angle θ_I are nonlinear functions of k, θ_H, the refractive indices, and ε. Because a greater correction is required at the outer wall of the hydrocyclone (greatest $|\varepsilon|$), observations in the corrections at the outer wall are used to determine trends in the results.

3.3 Procedure to Obtain Corrected Velocity Measurements

A procedure to properly obtain velocity measurements is outlined below.

TABLE 3.1.
The working equations for the axial corrections

$$X_{IX} = \frac{\left\{2\left[\frac{\cos\theta_H + \sin\theta_H \tan\left(\theta_H - \tilde{\theta}_{3A}\right)}{\tan\left(\theta_{3A} - \theta_H\right) + \tan\left(\theta_H - \tilde{\theta}_{3A}\right)}\right]\cos\theta_H - \left(\cos\theta_H + \sin\theta_H \tan\theta_{2B}\right)\sin\theta_H\right\}\epsilon\tan k}{\cos^2\theta_H - \sin^2\theta_H \tan^2\theta_{2B}} \qquad \text{(A)}$$

$$X_{IY} = 0 \qquad \text{(B)}$$

$$X_{IZ} = \left\{\left(\cos\theta_H + \sin\theta_H \tan\theta_{2B}\right) - 2\left[\frac{\cos\theta_H + \sin\theta_H \tan\left(\theta_H - \tilde{\theta}_{3A}\right)}{\tan\left(\theta_{3A} - \theta_H\right) + \tan\left(\theta_H - \tilde{\theta}_{3A}\right)}\right]\tan\left(\theta_{3A} - \theta_H\right)\right\}$$
$$\left\{\frac{\epsilon\cos\theta_H \tan k}{\cos^2\theta_H - \sin^2\theta_H \tan^2\theta_{2B}} + \frac{R}{2\left[\frac{\cos\theta_H + \sin\theta_H \tan\left(\theta_H - \tilde{\theta}_{3A}\right)}{\tan\left(\theta_{3A} - \theta_H\right) + \tan\left(\theta_H - \tilde{\theta}_{3A}\right)}\right] - \left(\cos\theta_H - \sin\theta_H \tan\theta_{2B}\right)\tan\theta_H}\right\} \qquad \text{(C)}$$

$$\theta_I = \left(\theta_{3A} - \tilde{\theta}_{3A}\right) / 2 \qquad \text{(D)}$$

where

$$\beta_2 \sin\theta_{2A} = \beta_3 \sin\theta_{3A} \qquad \text{(E)}$$

$$\beta_2 \sin\tilde{\theta}_{2A} = \beta_3 \sin\tilde{\theta}_{3A} \qquad \text{(F)}$$

$$\theta_{2A} = \theta_H + \theta_{2B} \qquad \text{(G)}$$

$$\tilde{\theta}_{2A} = \theta_H - \theta_{2B} \qquad \text{(H)}$$

$$\beta_1 \sin k = \beta_2 \sin\theta_{2B} \qquad \text{(I)}$$

TABLE 3.2.
The working equations for the tangential corrections

$$X_{IX} = -R\cos\theta_A - R\sin\theta_A \left\{ \frac{\frac{\beta_2}{\beta_3}\cos\theta_{2B} - \left(\frac{\beta_2}{\beta_3}\cos\theta_{2A} - \cos\theta_{3A}\right)\cos\theta_H\cos\theta_A}{\left(\frac{\beta_2}{\beta_3}\cos\theta_{2A} - \cos\theta_{3A}\right)\cos\theta_H\sin\theta_A - \frac{\beta_2}{\beta_3}\sin\theta_{2B}} \right\} \quad (J)$$

$$X_{IY} = 0 \quad (K)$$

$$X_{IZ} = R\sin\theta_A \left\{ \frac{\left(\frac{\beta_2}{\beta_3}\cos\theta_{2A} - \cos\theta_{3A}\right)\sin\theta_H}{\left(\frac{\beta_2}{\beta_3}\cos\theta_{2A} - \cos\theta_{3A}\right)\cos\theta_H\sin\theta_A - \frac{\beta_2}{\beta_3}\sin\theta_{2B}} \right\} \quad (L)$$

$$\cos\left(2\theta_I\right) = \left(\frac{\beta_2}{\beta_3}\right)^2\cos\left(2\theta_{2B}\right) - 2\,\frac{\beta_2}{\beta_3}\left(\frac{\beta_2}{\beta_3}\cos\theta_{2A} - \cos\theta_{3A}\right)\cos\theta_H\cos\left(\theta_A + \theta_{2B}\right)$$
$$+ \left(\frac{\beta_2}{\beta_3}\cos\theta_{2A} - \cos\theta_{3A}\right)^2\left[\cos^2\theta_H\cos\left(2\theta_A\right) + \sin^2\theta_H\right] \quad (M)$$

where $\beta_2\sin\theta_{2A} = \beta_3\sin\theta_{3A}$ (N)

$$\cos\theta_{2A} = \cos\theta_H\cos\left(\theta_A - \theta_{2B}\right) \quad (O)$$

$$\sin\theta_A - \cos\theta_A\tan\theta_{2B} = \frac{\epsilon}{R}\tan k \quad (P)$$

$$\beta_1\sin k = \beta_2\sin\theta_{2B} \quad (Q)$$

1. Focus the beams at the outer wall of the test section at the desired Z-position. This may be done visually using a ruler placed along the outer wall of the test section.
2. Move the test section laterally until the beams intersect at the inner wall of the hydrocyclone. Dabir (1983) discusses how to verify this.
3. Use the appropriate equation for X_{IX} in Chapter 3 to determine the distance the test section must be moved to position the point of intersection of the beams at the axis of symmetry of the hydrocyclone. This is done by setting X_{IX} equal to zero and solving for ε. The test section is then moved laterally this distance.
4. Use the proper equation for X_{IX} presented in Chapter 3 to determine the movement of the test section necessary to position the beams at the desired radial position.
5. The position of the corresponding axial position (X_{IZ}) of the measurement is obtained using the appropriate equation in Chapter 3.
6. The wavelength of the light in the test fluid is obtained from Equation 1.5.
7. The angle θ_I is then obtained using the appropriate equation in Chapter 3.
8. The fringe spacing is then calculated using Equation 1.2.

9. Finally, the velocity is determined from Equation 1.1 using the doppler frequency obtained from the measurement system.

If raw data in the form of ε vs $\langle f_d \rangle$ has already been obtained, the corrections are made using steps 4-9. An example of how to apply the correction is presented in Appendix C. Computer programs that may be used to generate the corrections in the position of measurement and the half-angle θ_I are presented in Appendix A.

3.4 Effect of the Refractive Indices

3.4.1 Effect on X_{IX}

For the axial measurements, the correction for X_{IX} is linear in ε. The axial correction is symmetric about the test section with respect to the $\pm\varepsilon$ movement of the test section. Also, maximum sensitivity in the X_{IX} measurement occurs when $\beta_2 > \beta_3$. The sensitivity also increases with increasing β_2:β_3 ratio (see Figure 3.1).

For the tangential measurements, the correction for X_{IX} is nonlinear in ε. When $\beta_2 > \beta_3$, maximum X_{IX} sensitivity is obtained when the test section is moved away from the laser (move negative ε), obtaining profiles in the half of the test section closest to the laser. When $\beta_2 < \beta_3$, maximum X_{IX} sensitivity is obtained when moving the test section in the positive ε direction (toward the laser). For this case ($\beta_2 < \beta_3$), there is greater sensitivity for all ε over the $\beta_2 > \beta_3$ case (see Figure 3.2).

3.4.2 Effect on X_{IZ}

As the β_2/β_3 ratio moves away from 1, the refraction in the z-direction increases. When $\beta_2 < \beta_3$, the refraction is in the positive

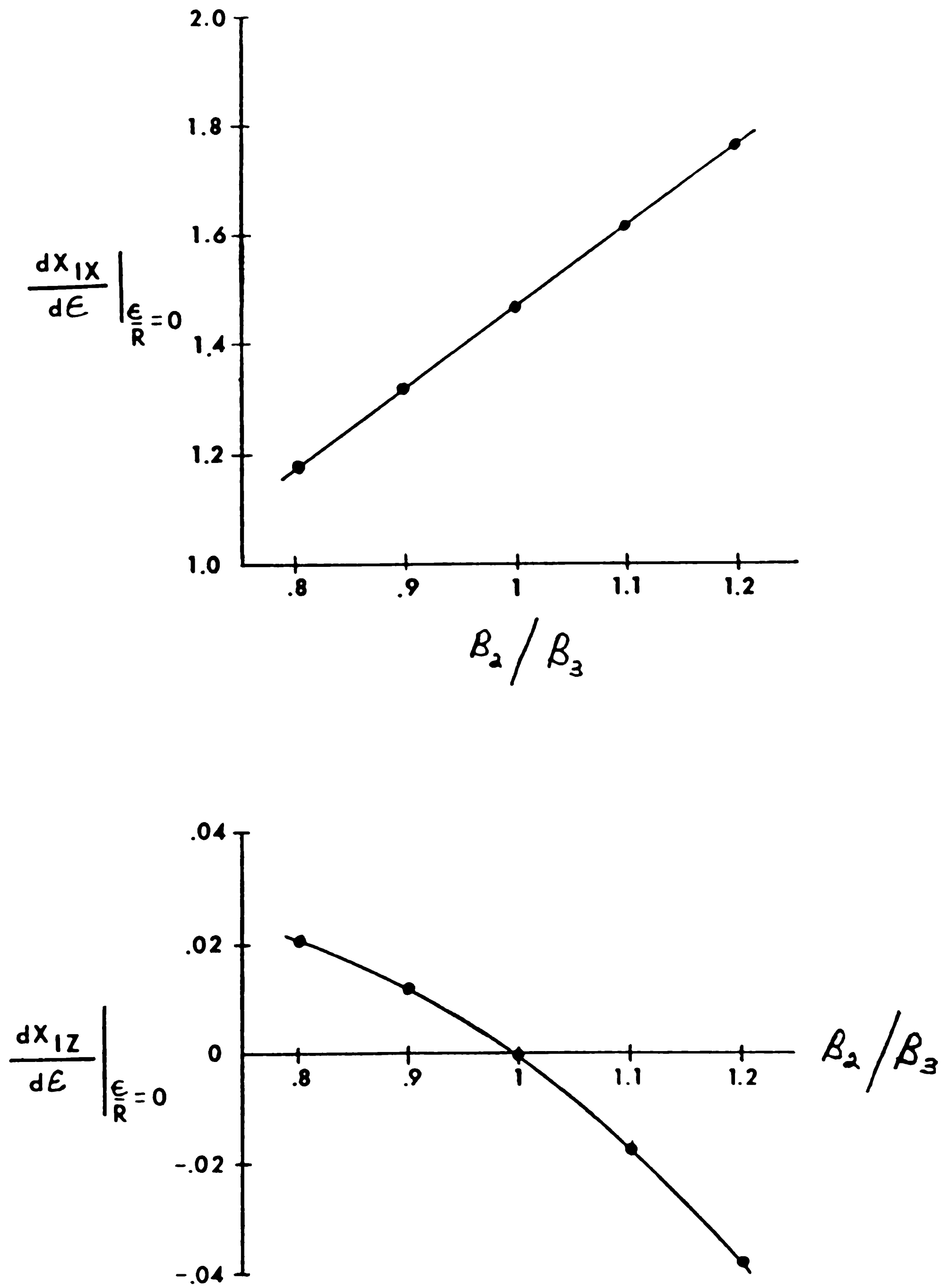

Figure 3.1 . Sensitivity of the corrections for axial measurements with respect to the refractive indices. (β_1/β_2 = 1/1.47, k = 5.71° , θ_H = 5.7°)

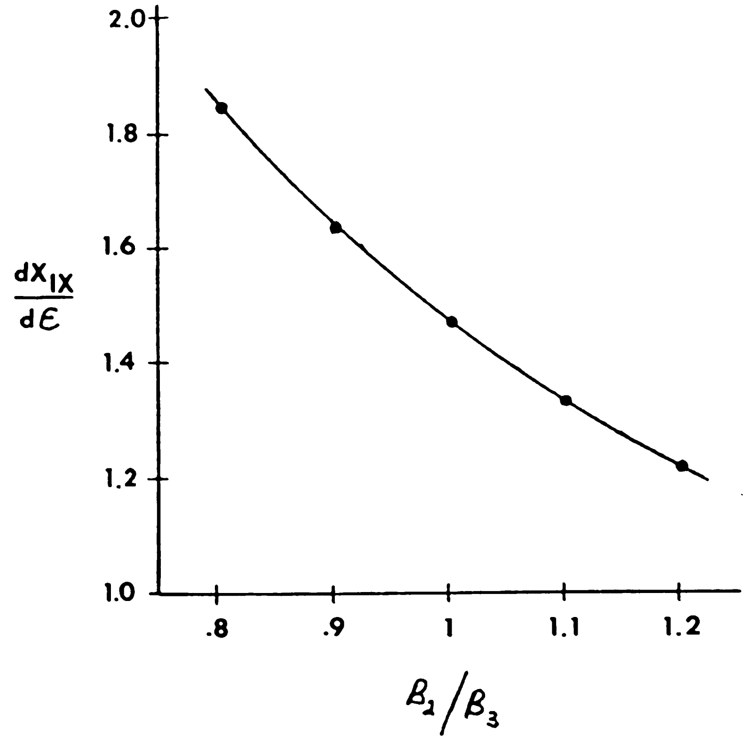

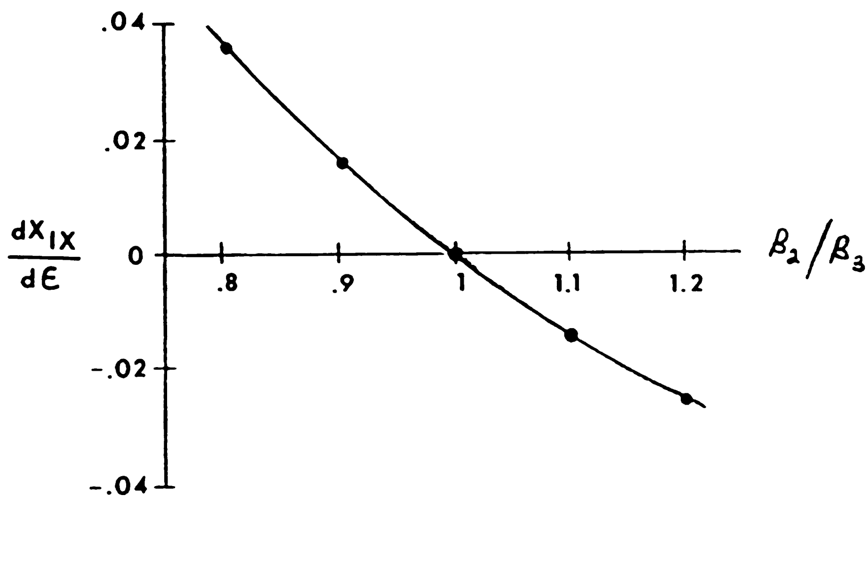

Figure 3.2 . Sensitivity of the corrections for tangential measurements with respect to the refractive indices. ($\beta_1/\beta_2 = 1/1.47$, $k = 5.71°$, $\theta_H = 5.7°$)

z-direction (above the optical bisector). When $\beta_2 > \beta_3$, refraction is in the negative z-direction (below the optical bisector).

3.5 Use of Small-Angle Approximations

Tables 3.3 and 3.4 present equations for the corrections for axial and tangential measurements that result from simplifying the equations in Table 3.1 and 3.2 using the small-angle linearizations for the angles ($\sin\theta \sim \theta$, $\cos\theta \sim 1$). The equations for X_{IX} and θ_I in Table 3.3 are the same equations as those derived by Dabir (1983). While his derivation for X_{IZ} is correct, an error was made in the presentation of the final equation. The correct equation for X_{IZ} is presented in Table 3.3.

The equations for the tangential corrections presented in Table 3.4 result from a rigorous derivation that is then simplified using the small-angle approximations. These equations are different from those presented by Dabir (1983). Dabir derives the correction for tangential measurements in a cylindrical geometry initially making the small-angle assumption for the angles (and then carrying out the derivation). Again, while his derivation is correct, the final presentation of the equation is incorrect. Dabir's equation should be

$$X_{IX} = \frac{\frac{\beta_2}{\beta_1}}{1 + \left(\frac{\beta_3 - \beta_2}{\beta_2}\right) \left(1 + \frac{\beta_2}{\beta_1} \frac{\varepsilon}{R}\right)} \qquad (3.1)$$

For corrections to tangential measurements in cylindrical geometries, either the above equation or the equation presented for X_{IX} in Table 3.4 may be used.

Dabir did not rigorously derive an equation for the corrections to tangential measurements in conical geometries. He assumed that the effect of θ_H on the refraction in the z-direction would be negligible ($X_{IZ} \sim 0$) due

TABLE 3.3.

The corrections for the axial measurements using small-angle approximations.

$$X_{IX} = \frac{\beta_3}{\beta_1} c \left\{ \frac{1 + \theta_H^{\,2} \left[1 - \frac{\beta_2}{\beta_3} \left(1 + \left(\frac{\beta_1}{\beta_2} k \right)^2 \right) \right]}{1 - \theta_H^{\,2} \left(\frac{\beta_1}{\beta_2} k \right)^2} \right\} \qquad \text{(R)}$$

$$X_{IZ} = \left\{ k\, \theta_H \left[\frac{\beta_1 \left(\beta_3 - \beta_2 \right)}{\beta_2\, \beta_3} \right] + \frac{\theta_H}{k} \left[\frac{\beta_3 - \beta_2}{\beta_1} \right] + \frac{\theta_H^{\,3}}{k} \left[\frac{\left(\beta_2 - \beta_3 \right)^2}{\beta_1\, \beta_3} \right] \right\} \qquad \text{(S)}$$

$$\left\{ \frac{c\, k}{1 - \theta_H^{\,2} \left(\frac{\beta_1}{\beta_2} k \right)^2} + \frac{R}{\frac{\beta_3}{\beta_1 k} + \theta_H^{\,2} \left[\frac{\beta_3 - \beta_2}{\beta_1 k} + \frac{\beta_1}{\beta_2} k \right]} \right\}$$

$$\theta_I = \frac{\beta_1}{\beta_3} k \qquad \text{(T)}$$

TABLE 3.4.

The corrections for the tangential measurements using the small-angle aproximations.

$$X_{IX} = -R - R\left(\frac{\beta_1}{\beta_2} + \frac{\varepsilon}{R}\right)\left\{\frac{1}{\left(\frac{\beta_2}{\beta_3} - 1\right)\left(\frac{\beta_1}{\beta_2} + \frac{\varepsilon}{R}\right) - \frac{\beta_1}{\beta_3}}\right\} \quad (U)$$

$$X_{IZ} = R\left(\frac{\beta_1}{\beta_2} + \frac{\varepsilon}{R}\right)\left\{\frac{\left(\frac{\beta_2}{\beta_3} - 1\right)\theta_H}{\left(\frac{\beta_2}{\beta_3} - 1\right)\left(\frac{\beta_1}{\beta_2} + \frac{\varepsilon}{R}\right) - \frac{\beta_1}{\beta_3}}\right\} \quad (V)$$

$$\cos\left(2\theta_I\right) = \left(\frac{\beta_2}{\beta_3}\right)^2 \cos\left(2\frac{\beta_1}{\beta_2}k\right) - 2\frac{\beta_2}{\beta_3}\left(\frac{\beta_2}{\beta_3} - 1\right)\cos\left(2\frac{\beta_1}{\beta_2} + \frac{\varepsilon}{R}\right)k + \left(\frac{\beta_2}{\beta_3} - 1\right)^2\left[\cos\left(\frac{\beta_1}{\beta_2} + \frac{\varepsilon}{R}\right)2k + \theta_H\right] \quad (W)$$

to the small-angle assumption. For the system used by Dabir, this assumption is valid. He did, however, include the effect of θ_H in his calculation of X_{IX} by modifying the radius as follows:

$$R = Z \tan \theta_H \sim Z \theta_H \tag{3.2}$$

Unfortunately, this overexaggerates the effect of the slant of the hydrocyclone wall (θ_H), producing errors in X_{IX}. For the system studied by Dabir, errors in excess of 20% resulted.

The range in θ_H and k for which the small-angle approximations remain valid was examined. The refractive indices of the system were chosen to be those of air, glass, and water respectively. These media are typical of experimental systems. For k up to 25 degrees, the error in the position by using the small angle approximation (sin k = k, cos k = 1) is under 5%. For the range of θ_H up to 22.5^o, the error incurred in the position by using the small-angle approximation is under 5%.

3.6 Conclusions

3.6.1 Design of an Experiment

For axial measurements, the test section should be designed with $\beta_2 > \beta_3$. This provides maximum sensitivity of the measurements.

For tangential measurements, the test section should be designed with $\beta_2 < \beta_3$ for maximum sensitivity of the measurement. Also, for the tangential measurements, the measurements should be made on the side of the test section closest to the laser for maximum sensitivity in the measurements (see Figure B.1).

For cases where both types of measurements must be made, the refractive indices of mediums 2 and 3 should be chosen to be as similar as possible. While a trade-off in the sensitivities of the two types of measurements exists, this will minimize the refraction in the z-direction.

Making the measurements on the side of the test section closest to the laser will also minimize the refraction in the z-direction (see Appendix B).

3.6.2 Finding the Axis of the Hydrocyclone

In the past, profiles were made by starting from the wall of the hydrocyclone and moving across the hydrocyclone, or by finding where the maximum or minimum occurs in the velocity profile and calling that point the center (or axis). Velocity measurements across a radius were made by assuming symmetry. Unfortunately, there is no conclusive evidence to indicate that the velocity profiles within the hydrocyclone should be symmetric about the axis of symmetry (although various flow visualization studies appear to indicate this); thus, there may be error in assuming that the point of inflection in the velocity profiles (either axial or tangential) always occurs at the center of the hydrocyclone.

The following alternative procedure should be used to position the intersection of the beams at the axis of the hydrocyclone. Dabir (1983) discusses how to verify that the beams actually intersect at the wall. He also discusses how to align the beams and verify that they are in the proper optical plane. Equations (A) or (J) may then be used to locate the axis of the hydrocyclone by determining the ε that corresponds to the distance the test section must be moved to be at the center of the hydrocyclone. The test section is then moved the specified amount, positioning the beams at the axis of the hydrocyclone.

3.7 Recommendations

The present study allows one to determine the position of the measurement with respect to the movement of the test section. Thus, one moves the test section and then determines where the measuring point is. It is desired to be able to choose the location of measurement (both radial position and axial position) and then adjust the test section so that the position is obtained.

The set-up examined allows measurements to be obtained across a radius by moving the test section with the use of a milling table (see Figure 2.2). While the results of this study permit measurements at particular points across a radius, the measurements may not be located in the same z-plane. Although results indicate that the z-refraction in most cases is small, it is still preferred to be able to make measurements at the exact location desired. To do this, adjustment of the axial position (z-position) of the beams is necessary. The milling table provides such an adjustment to be made. The analytical changes to the corrections developed occur in the X_{FX} vector that describes the position of the origin with respect to the fictitious focal point F. To allow for 2-dimensional movement of the test section, the vector $\underline{X}_F$ should be written as follows:

$$\underline{X}_F = \underline{X}^o{}_F + \varepsilon_X \underline{e}_X + \varepsilon_Z \underline{e}_Z \qquad (3.3)$$

where ε_X accounts for the radial movement of the test section and ε_Z accounts for the axial movement of the test section. The corrections should then be developed with this modification. The end result will allow one to pick a particular radial and axial position and determine the necessary movement in ε_X and ε_Z to attain that position. This will allow profiles to be obtained in the same axial plane (z-plane).

APPENDIX A

COMPUTER PROGRAMS

LIST OF COMPUTER NOTATION

B1 = refractive index of medium 1

B2 = refractive index of medium 2

B3 = refractive index of medium 3

RT = radius at top of hydrocyclone

RB = radius at apex of hydrocyclone

HL = length of conical section

R = radius at optical bisector

Z = Z-position of optical bisector

A1 = k

A2 = θ_H

A3 = θ_{2B}

A4 = θ_{2A}

A5 = θ_{3A}

A6 = $\tilde{\theta}_{2A}$

A7 = $\tilde{\theta}_{3A}$

A8 = θ_I

N = number of increments across a radius

E = ε

EL = lower bound of ε

FO = X^o_{FX}

F = X_{FX}

XIX = X_{IX}

XIZ = X_{IZ}

VX = ℓ_{3X}

VY = ℓ_{3Y}

VZ = ℓ_{3Z}

VXT = $\tilde{\ell}_{3X}$

VYT = $\tilde{\ell}_{3Y}$

VZT = $\tilde{\ell}_{3Z}$

PI = 3.141529

S1,S2,S3,S4,S5,S6,A,B = storage variables for intermediate calculations

Table A.1. Relevant parameters for the computer programs

β_1
β_2
β_3
k
Z
RT
RB
HL

Table A.2 . Flow chart of computer program used to develop corrections for axial measurements.

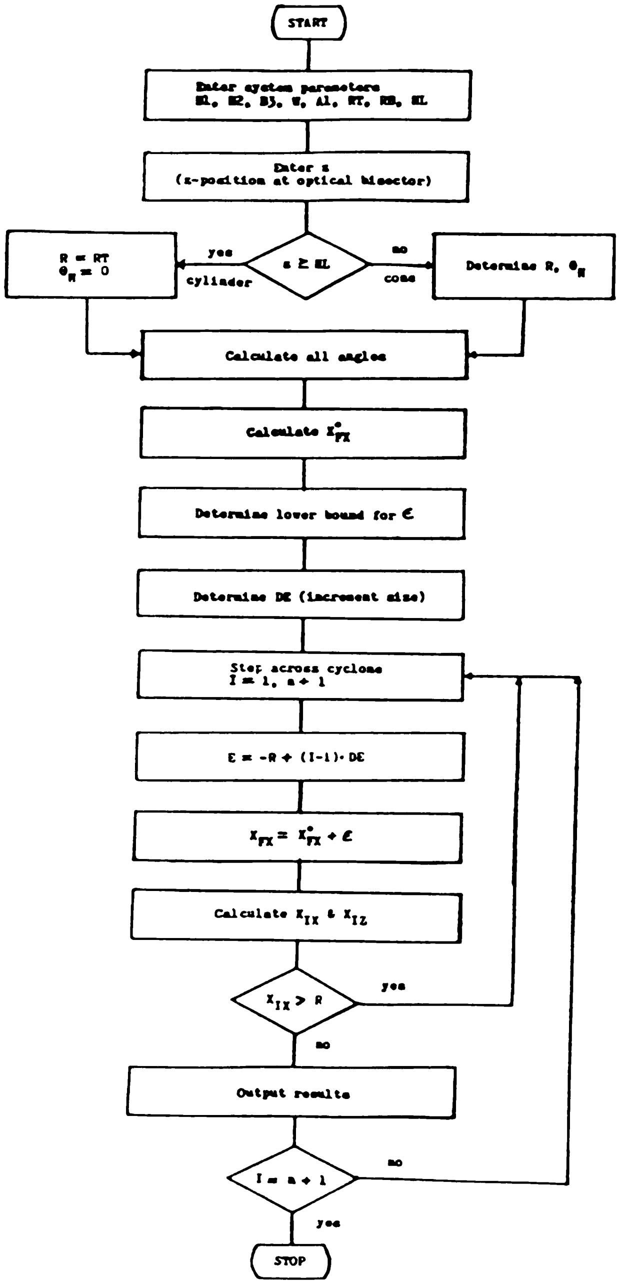

Table A.3. Computer program used to generate corrections for axial measurements.

```
          PROGRAM REF(INPUT,OUTPUT,TAPE5=INPUT,TAPE6,=OUTPUT)
C
C         ENTER PARAMETERS
          DATA B1, B2, B3/1.0,1.47,1.33348/
          DATA W/60/
          DATA A1/5.71/
          DATA RT,RB,HL/38.,6.08,320./
          PI = 3.141529
C
          WRITE(6,9)
 9        FORMAT(2X,"AXIAL CORRECTIONS"/)
C
C         ENTER Z-POSITION AT OPTICAL BISECTOR IN MM
          READ *, Z
C
C         CALCULATE R AT OPTICAL BISECTOR
          IF (Z .LT. HL) GO TO 3
          R = RT
          A2 = 0.0
          WRITE(6,499) Z,R
 499      FORMAT(2X,"CYLINDRICAL SECTION",10X,"Z = ",F7.3,10X,
         $"R = ",F7.3/)
          GO TO 5
 3        ZO = RB * HL / (RT - RB)
          R = RT * ( (Z + ZO) / (HL + ZO) )
          A2 = ATAN( RT / (HL + ZO) ) * (180./PI)
C
C         OUTPUT SYSTEM PARAMETERS
          WRITE(6,599) Z, R
 599      FORMAT(2X,"CONICAL SECTION",10X,"Z = ",F7.3,10X,"R = ",F7.3/)
 5        WRITE(6,199) B1,B2,B3,RT,RB,HL,A1,A2,W
 199      FORMAT(32X,"B1 = ",F6.3,6X,"B2 = ",F6.3,6X,"B3 = ",F6.3/,32X,
         $ "RT = ",F7.2,5X,"RB = ",F7.2,5X,"HL = ",F7.2/,32X,"THETAK =",
         $ F5.2,3X,"THETAH = ",F5.2,3X,"W = ",F7.2/)
          WRITE(6,799)
 799      FORMAT(20X,"E",10X,"THETAI",7X,"XIX",9X,"XIZ"/)
          WRITE(6,899)
 899      FORMAT(91("*")/)
C
C         CALCULATE ANGLES
          A1 = A1 * (PI/180)
          A2 = A2 * (PI/180.)
          A3 = ASIN( B1/B2 * SIN(A1) )
          A4 = A2 + A3
          A5 = ASIN( B2/B3 * SIN(A4) )
          A6 = A2 - A3
          A7 = ASIN( B2/B3 * SIN(A6) )
          A8 = (A5 - A7) / 2.
          A8 = A8 * (180./PI)
```

COMPUTER PROGRAM

```
C
C          CALCULATE FO
           S1 = COS(A2) - SIN(A2) * TAN(A3)
           S2 = COS(A2) + SIN(A2) * TAN(A3)
           S3 = ( COS(A2) + SIN(A2) * TAN(A2-A7) ) / ( TAN(A5-A2) +
          $ TAN(A2-A7) )
           S4 = (R * S1 * S2) + ( (W-R) * TAN(A3) ) * ( -S2 * SIN(A2) +
          $S2 * S3 + S3 * S1 )
           S5 = TAN(A1) * ( S2 * S3 + S3 * S1 - S2 * SIN(A2) )
           FO = S4/S5 - W
C
C          CALCULATE THE COMPONENTS OF THE POSITION VECTOR AS TRAVERSE
C          THE HYDROCYCLONE
C          ENTER THE NUMBER OF EQUALLY SPACED MEASUREMENTS ACROSS A
           RADIUS
           N = 10
C
C          DETERMINE LOWER BOUND FOR E
           EL = (W-R) * (TAN(A3)/TAN(A1)) - W - FO
C
C          DETERMINE SIZE OF INCREMENT
           DE = EL/N
C
C          STEP ACROSS HYDROCYCLONE
           DO 10 I=1,3*N
           E = EL + (I-1)*DE
           F = FO + E
C
C          CALCULATE THE COMPONENTS OF THE POSITION VECTOR
           S6 = ( (W+F) * TAN(A1) - (W-R) * TAN(A3) )
           XIX = -R -S6/S1 * SIN(A2) + S6 * S3 * (1./S1 + 1./S2)
           XIZ = S6/S1 * COS(A2) - S6 * S3 * (1./S1 + 1./S2) * TAN(A5-A2)
           IF ( ABS(XIX) .GT. R ) GO TO 10
C
C          OUTPUT RESULTS
           WRITE(6,999) E, A8, XIX, XIZ
 999       FORMAT(18X,F7.3,5X,F6.3,5X,F7.3,5X,F7.3)
  10       CONTINUE
           WRITE(6,299)
 299       FORMAT(/,4X,"ALL POSITIONS IN MM AND ALL ANGLES IN DEGREES"/)
           STOP
           END
```

Table A.4 . Flow chart of computer program used to develop corrections for tangential measurements.

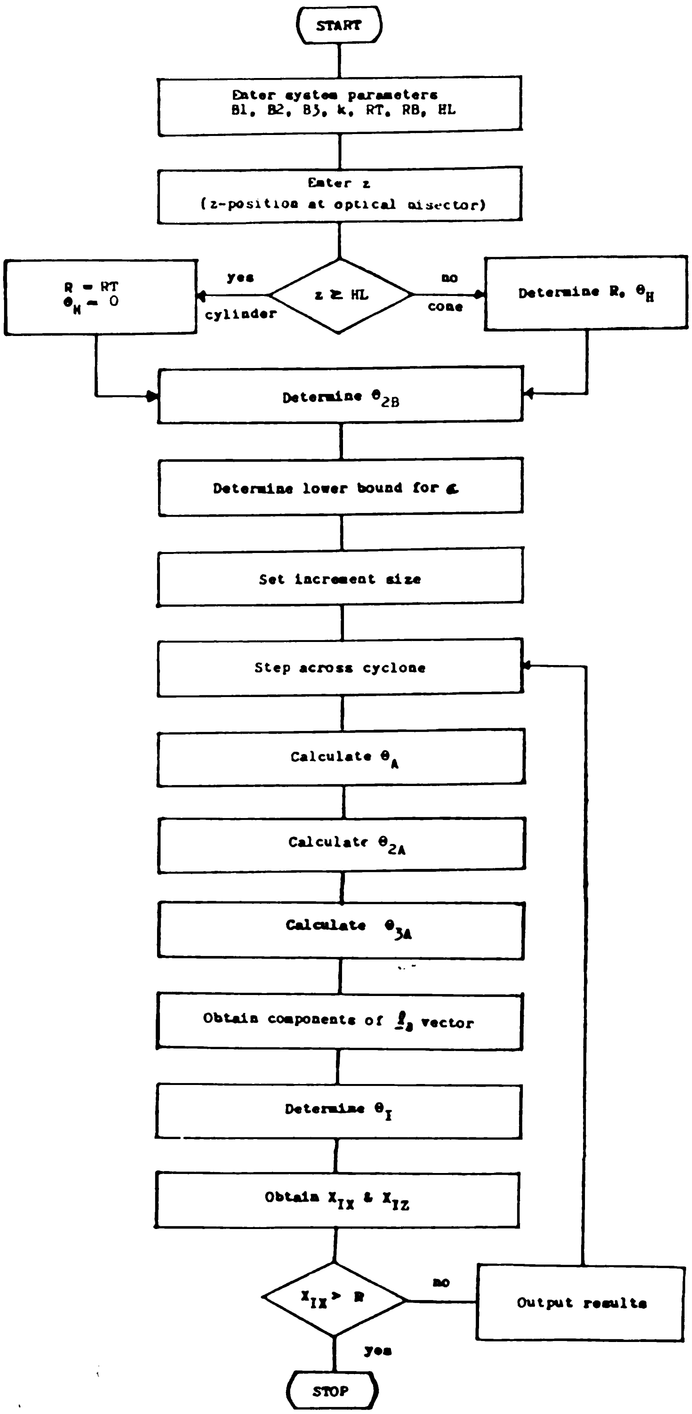

Table A.5. Computer program used to generate corrections for tangential measurements.

```
      PROGRAM REF(INPUT,OUTPUT,TAPE5=INPUT,TAPE6=OUTPUT)
C
C     ENTER PARAMETERS
      DATA B1,B2,B3/1.0,1.47,1.33348/
      DATA RT,RB,HL/38.,6.08,320./
      DATA A1/5.71/
      DATA EPS / 1.0E-5 /
      PI = 3.141529
C
      WRITE(6,9)
  9   FORMAT(2X,"TANGENTIAL CORRECTIONS"/)
C
C     ENTER Z-POSITION AT OPTICAL BISECTOR IN MM
      READ *, Z
C
C     CALCULATE R AT OPTICAL BISECTOR
      IF ( Z .LT. HL ) GO TO 3
      R = RT
      A2 = 0.0
      WRITE(6,499) Z, R
 499  FORMAT (2X,"CYLINDRICAL SECTION",10X,"Z = ",F7.3,10X,
     $ "R = ",F7.3/)
      GO TO 5
  3   ZO = RB * HL / (RT - RB)
      R = RT * ( (Z + ZO) / (HL + ZO) )
      A2 = ATAN( RT/(HL + ZO) ) * (180./PI)
C
C     OUTPUT SYSTEM PARAMETERS
      WRITE(6,599) Z,R
 599  FORMAT(2X,"CONICAL SECTION",10X,"Z = ",F7.3,10X,"R = ",F.3/)
  5   WRITE(6,199) B1,B2,B3,RT,RB,HL,A1,A2
 199  FORMAT(32X),"B1 = ",F6.3,6X,"B2 = ",F6.3,6X,"B3 = ",F6.3/,32X,
     $ "RT = ",F7.2,5X,"RB = ",F7.2,5X,"HL = ",F7.2/32X,"THETAK =",
     $ F5.2,3X,"THETAH = ",F5.2/)
      WRITE(6,799)
 799  FORMAT(18X,"E",10X,"THETAI",7X,"XIX",9X,"XIZ"/)
      WRITE(6,899)
 899  FORMAT(85("*")/)
      A1 = A1 * (PI/180.)
      A2 = A2 * (PI/180.)
C
C     DETERMINE THETA2B - (A3)
      A3 = ASIN( B1/B2 * SIN(A1) )
C
C     DETERMINE LOWER BOUND FOR E
      EL = -R * TAN(A3)/TAN(A1)
C
C     ENTER THE NUMBER OF EQUALLY SPACED MEASUREMENTS ACROSS A
C     RADIUS
```

```
      N = 10
C
C     DETERMINE SIZE OF INCREMENT
      DE = -EL/N
C
C     PROCEED TO STEP ACROSS HYDROCYCLONE
      DO 10 I=1,5*N
      E = EL + (I-1) * DE
C
C     DETERMINE THETAA - (A9)
      GUESS = A3
 20   A9 = ABS( ASIN( COS(GUESS)*TAN(A3) + E*TAN(A1)/R) )
      IF ( ABS(GUESS-A9) .LT. EPS ) GO TO 40
      GUESS = A9
      GO TO 20
 40   IF ( E .GT. (R/TAN(A1)) ) A9 = PI -A9
C
C     DETERMINE THETA2A - (A4)
      S1 = COS(A2) * ( COS(A3) * COS(A9) + SIN(A3) * SIN(A9) )
      A4 = ABS( ACOS(S1) )
C
C     CHECK FOR REFLECTION
      IF (B3 .GT. B2) GO TO 42
      S5 = ASIN( B2/B3 )
      IF (A4 .GE. S5) GO TO 80
C
C     DETERMINE THETA3A - (A5)
 42   A5 = ASIN(B2/B3 * SIN(A4) )
C
C     CALCULATE THE COMPONENTS OF THE VECTORS DESCRIBING THE PATHS
C     OF THE BEAMS THROUGH THE HYDROCYCLONE
      IF ( A4 .EQ. 0. ) THEN
      A = 0.
      GO TO 45
      END IF
      A = ABS(SIN(A5) / SIN(A4) )
 45   B = A * COS(A4) - COS(A5)
      VX = A * COS(A3) - B * COS(A2) * COS(A9)
      VY = -A * SIN(A3) + B * COS(A2) * SIN(A9)
      VZ = -B * SIN(A2)
      VXT = VX
      VYT = -VY
      VZT = VZ
C
C     DETERMINE THETAI - (A8)
      S2 = VX * VXT + VY * VYT + VZ * VZT
      A8 = ACOS(S2) / 2.
      A8 = A8 * (180./PI)
C
C     CALCULATE THE COMPONENTS OF THE POSITION VECTOR
      XIX = ( - R * COS(A9) ) - ( R * SIN(A9)/VY ) * VX
      XIZ = -VZ * ( R * SIN(A9)/VY )
 75   IF (XIX .GT. R ) GO TO 100
```

```
C
C          OUTPUT RESULTS
           WRITE(6,999) E, A8, XIX, XIZ
 999       FORMAT(15X,F7.3,5X,F6.3,5X,F7.3,5X,F7.3)
  10       CONTINUE
  15       WRITE(6,299)
 299       FORMAT(/,4X,"ALL POSITIONS IN MM AND ALL ANGLES IN DEGREES"/)
           GO TO 100
  80       WRITE(6,99)
  99       FORMAT(/,4X,"TOTAL REFLECTION OCCURS"/)
 100       STOP
           END
```

APPENDIX B

SAMPLE COMPUTER OUTPUT

TABLE B.1.

Sample Computer Output of Corrections for Axial Measurements

Axial Corrections			
Conical Section	Z = 200.000	R = 26.030	
	B1 = 1.000	B2 = 1.470	B3 = 1.333
	RT = 38.00	RB = 6.08	HL = 320.00
	THETAK = 5.71	THETAH = 5.70	W = 60.00
E	THETAI	XIX	XIZ
-19.521	4.284	-26.030	.000
-17.569	4.284	-23.427	-.027
-15.617	4.284	-20.824	-.054
-13.665	4.282	-18.221	-.081
-11.713	4.284	-15.618	-.108
-9.761	4.284	-13.015	-.135
-7.808	4.284	-10.412	-.162
-5.856	4.284	-7.809	-.189
-3.904	4.284	-5.206	-.216
-1.952	4.284	-2.603	-.243
.000	4.284	.000	-.270
1.952	4.284	2.603	-.297
3.904	4.284	5.206	-.324
5.856	4.284	7.809	-.351
7.808	4.284	10.412	-.378
9.761	4.284	13.015	-.405
11.713	4.284	15.618	-.432
13.665	4.284	18.221	-.460
15.617	4.284	20.824	-.487
17.569	4.284	23.427	-.514
19.521	4.284	26.030	-.541

All positions in mm and all angles in degrees.

TABLE B.2.

Sample Computer Output of Corrections for Tangential Measurements

Tangential Corrections
Conical Section Z = 200.000 R = 26.030

B1 = 1.000 B2 = 1.470 B3 = 1.333
RT = 38.00 RB = 6.08 HL = 320.00
THETAK = 5.71 THETAH = 5.70

E	THETAI	XIX	XIZ
-17.660	4.279	-26.030	-.000
-15.894	4.239	-23.648	-.024
-14.128	4.199	-21.220	-.049
-12.362	4.159	-18.745	-.075
-10.596	4.119	-16.222	-.100
-8.830	4.079	-13.650	-.127
-7.064	4.040	-11.028	-.154
-5.298	4.000	-8.353	-.181
-3.532	3.960	-5.624	-.209
-1.766	3.920	-2.841	-.237
0.000	3.881	0.000	-.266
1.766	3.841	2.899	-.296
3.532	3.801	5.859	-.326
5.298	3.761	8.881	-.357
7.064	3.722	11.968	-.388
8.830	3.682	15.122	-.420
10.596	3.642	18.344	-.453
12.362	3.602	21.638	-.487
14.128	3.562	25.005	-.521

All positions in mm and all angles in degrees.

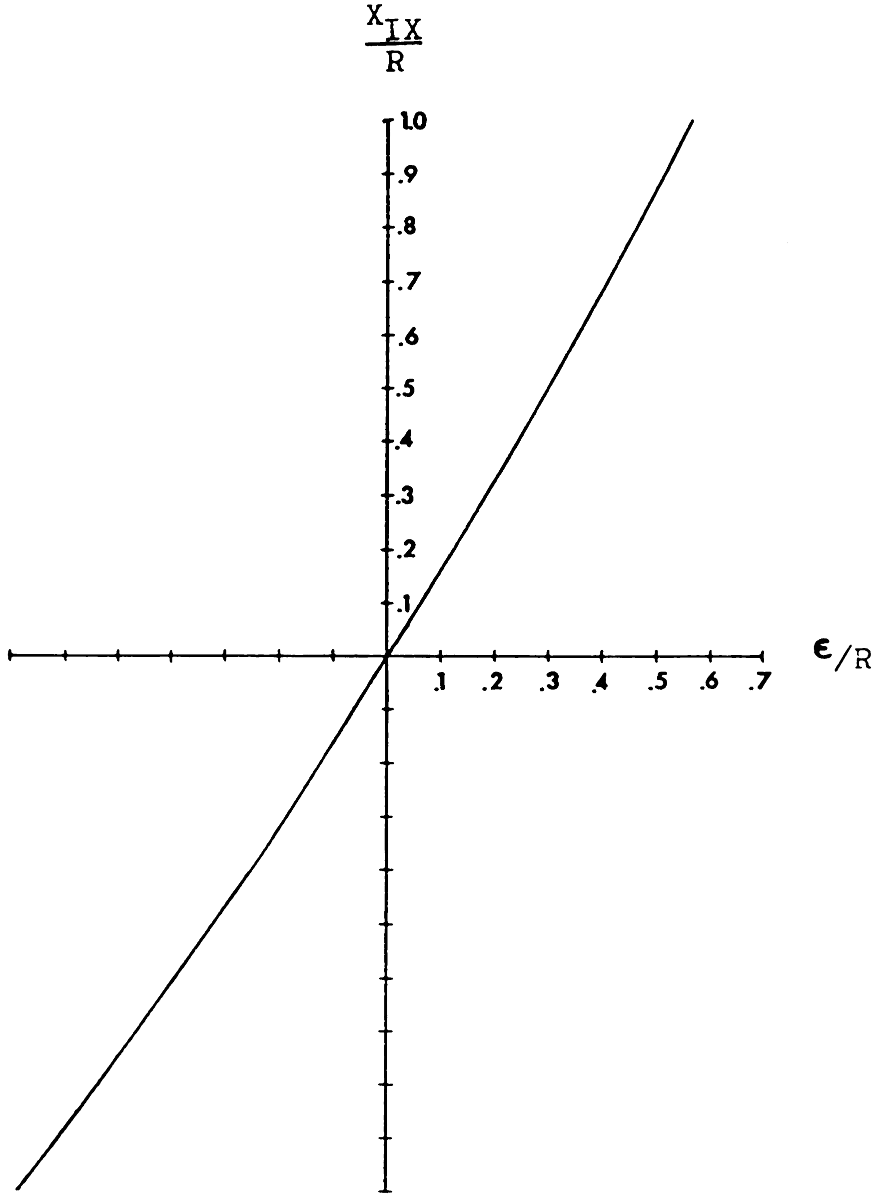

Figure B.1 . Corrections in the radial position for tangential measurements.

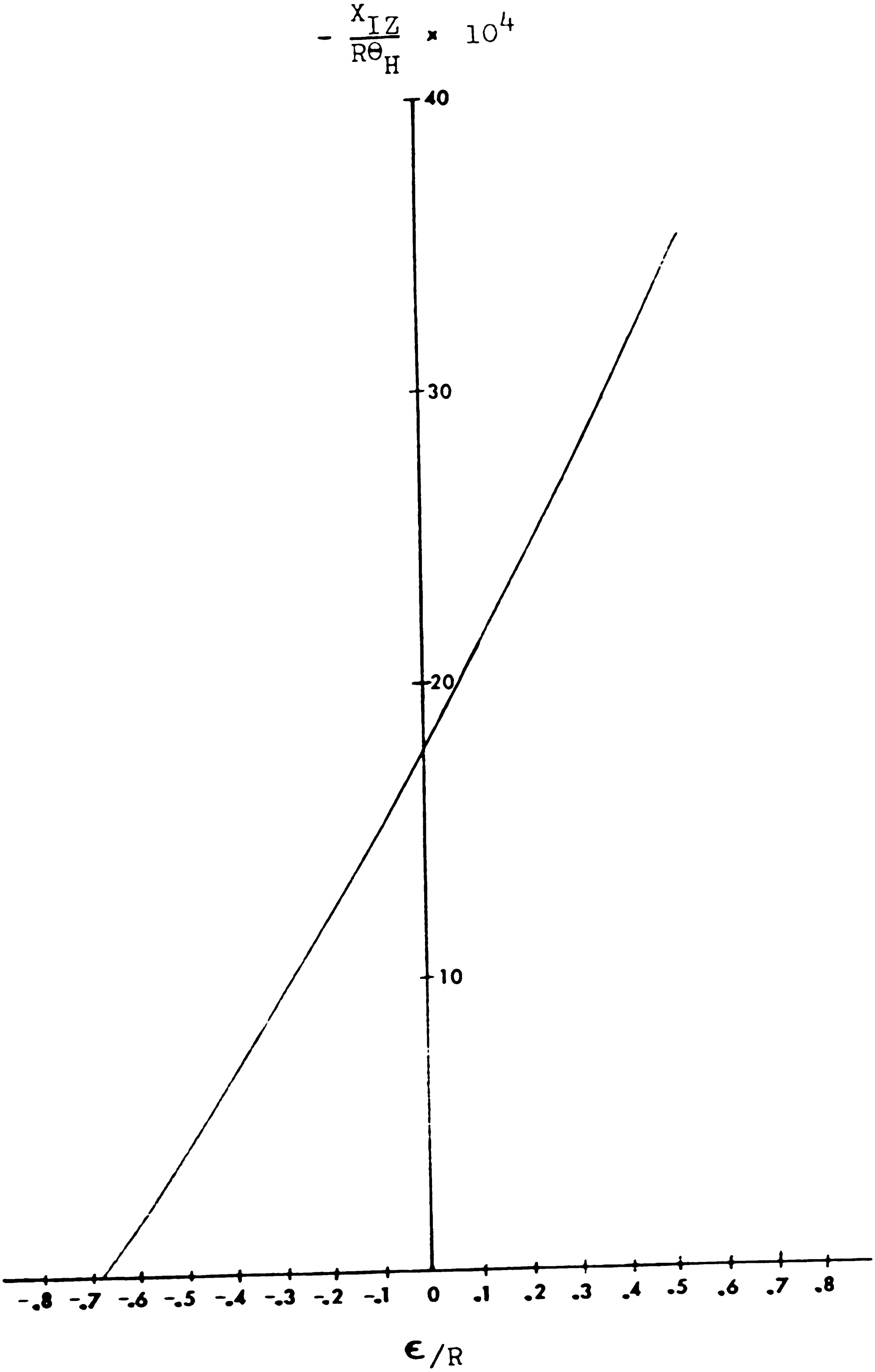

Figure B.2 . Corrections in the axial position for tangential measurements.

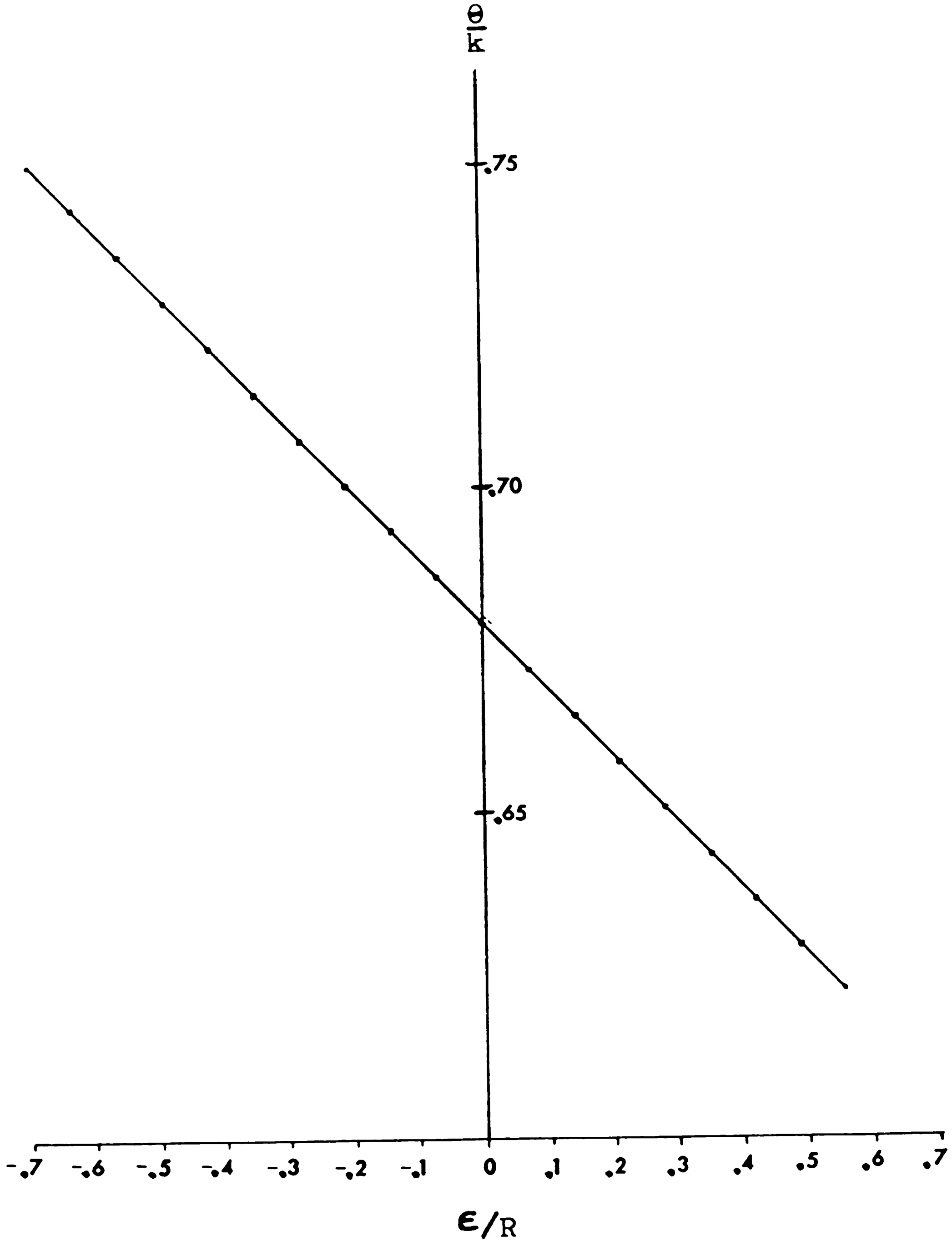

Figure B.3 . Corrections in the half-angle for tangential measurements.

APPENDIX C

ILLUSTRATION OF THE CORRECTIONS

APPENDIX C

ILLUSTRATION OF THE CORRECTIONS

Illustration of the Corrections

An illustration of the position and velocity corrections is presented in this appendix. The system examined is the one used by Dabir (1983) in his hydrocyclone studies. This system was chosen because it is considered a typical experimental system in that the laser sits in air, the hydrocyclone is made of glass, and the test fluid is water. The box is constructed of plexiglass with the same index of refraction of the glass ($\beta \simeq 1.47$). The space between the box and the hydrocyclone is filled with glycerine, also of refractive index of the glass. The hydrocyclone is constructed to Rietema's specifications (Rietema, 1961). The dimensions of the hydrocyclone are presented in Figure C.1. The laser system used is a TSI H_e-N_e laser ($\lambda = 632.8$ nm) with a lens that focuses the beams with a 5.71^o half-angle of intersection.

The relevant parameters for the computer programs (presented in Appendix A) are the refractive indices (β_1, β_2, β_3), the half-angle of the incident beams (k), the radial dimensions of the hydrocyclone at the top and apex (RT and RB), and the length of the conical section (HL). The dimensions of these parameters are presented in Table C.1. The output to the computer programs is presented in Appendix B. The corrections are presented in a nondimensionalized form in Figures B.1 - B.3.

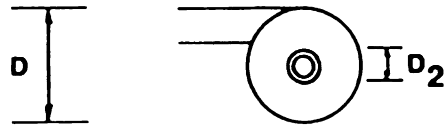

Dimension	This Study	Rietema [1961]
D	76 mm	76 mm
D_1	0.28 D	0.28 D
D_2	0.34 D	0.34 D
D_3	0.16 D	--
H_1	5 D	5 D
H_2	0.67 D	--
H_3	0.4 D	0.4 D
θ	11.3°	--

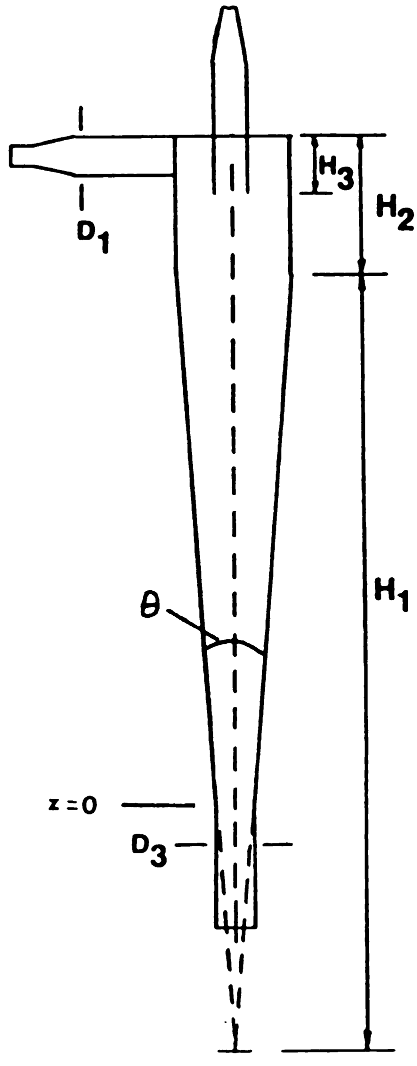

Figure C.1 . Dimensions of the hydrocyclone used in the study (nominal lengths given in mm).

Table C.1. Relevant parameters of the experimental system required by the computer programs in Appendix A to generate the corrections in the measurements.

β_1 = 1.00
β_2 = 1.47
β_3 = 1.333
k = 5.71°
Z = position = 200 mm
RT = 38 mm
RB = 6.08 mm
HL = 320 mm

The corrections influence both the location of the measurement and the velocity measurement itself. From Equation (D) in Table 3.1 it can be seen that θ_I is independent of position for axial measurements. It follows from Equation (1.2) that $d_F(\underline{x})$ is independent of position. d_F is dependent upon the wavelength of the light in the test fluid. The wavelength of the light is dependent upon the refractive indices of the media through which the light beams traverse (see Equation 1.5). Thus from Equation 1.1, the magnitude of the velocity is implicitly dependent on the refractive indices of the media through which the light beams pass. Also, from Equations (A) and (C) in Table 3.1 it can be seen that the refraction has changed the position of measurement. A sample of Dabir's raw data along with the corrected results for axial velocity measurements are presented in Table C.2. The results are plotted in Figure C.2.

For tangential measurements, it can be seen from Equations (M) - (P) that θ_I and therefore d_f is dependent on the position of the measurement. From Equations (J) and (L) in Table 3.2 it can be seen that the measuring point is also dependent on ε. Therefore for tangential measurements, the refraction phenomenon changes both the magnitude of the velocity and the position of the measurement.

A sample of Dabir's raw data for tangential velocity measurements along with the corrected results are presented in Table C.2. The results are plotted in Figure C.3.

Table C.2. Raw data and corresponding axial velocity measurements in a hydrocyclone.

raw data *		velocity measurement	
E (mm)	$f_d(\underline{X})$ (MH_z)	X_{IX} (mm)	$\langle U_Z \rangle$ (m/s)
0.00	-.1559	0.0	-.4952
0.51	-.1448	.68	-.4602
1.27	-.1089	1.694	-.346
2.29	-.1606	3.054	-.051
3.37	.1058	4.494	.3362
4.32	.2125	5.761	.6753
5.34	.2472	7.121	.7853
6.87	.1880	9.161	.5973
8.90	.1030	11.868	.3271
10.94	.0397	14.588	.1261
12.97	-.0066	17.295	-.021
15.00	-.0598	20.003	-.1901
17.04	-.0614	22.723	-.1951

* Dabir's data for the following conditions: Z (20; 15.3; 4), Re_F = 24,400.

Table C.3. Raw data and corresponding tangential velocity measurements in a hydrocyclone.

raw data *		corrected measurements			
E (mm)	f_d (MH_Z)	X_{IX} (mm)	θ_I (^{o})	d_f (μm)	U_θ (m/s)
0.0	.003	0.0	3.8828	3.505	.0105
0.51	.145	.781	3.8714	3.516	.5098
1.02	.304	1.718	3.8588	3.527	1.072
1.52	.395	2.525	3.8485	3.536	1.397
2.03	.474	3.306	3.8354	3.548	1.682
2.54	.518	4.100	3.8228	3.560	1.844
3.05	.542	4.842	3.8114	3.571	1.935
3.56	.548	5.831	3.803	3.579	1.961
4.06	.551	6.638	3.7914	3.590	1.978
5.59	.509	9.423	3.7446	3.634	1.850
6.60	.471	11.271	3.7343	3.644	1.716
7.62	.441	13.015	3.7144	3.663	1.616
8.64	.402	14.863	3.6858	3.692	1.484
9.65	.379	16.659	3.6601	3.718	1.409
10.67	.352	18.481	3.6401	3.739	1.316
11.68	.332	20.303	3.6144	3.765	1.250
12.70	.327	22.126	3.5916	3.789	1.239
13.72	.312	24.104	3.5705	3.811	1.189
14.73	.24	26.03	3.5459	3.838	.921

* Dabir's data for the following conditions: θ(20; 10.3; 4), Re_f = 20,100.

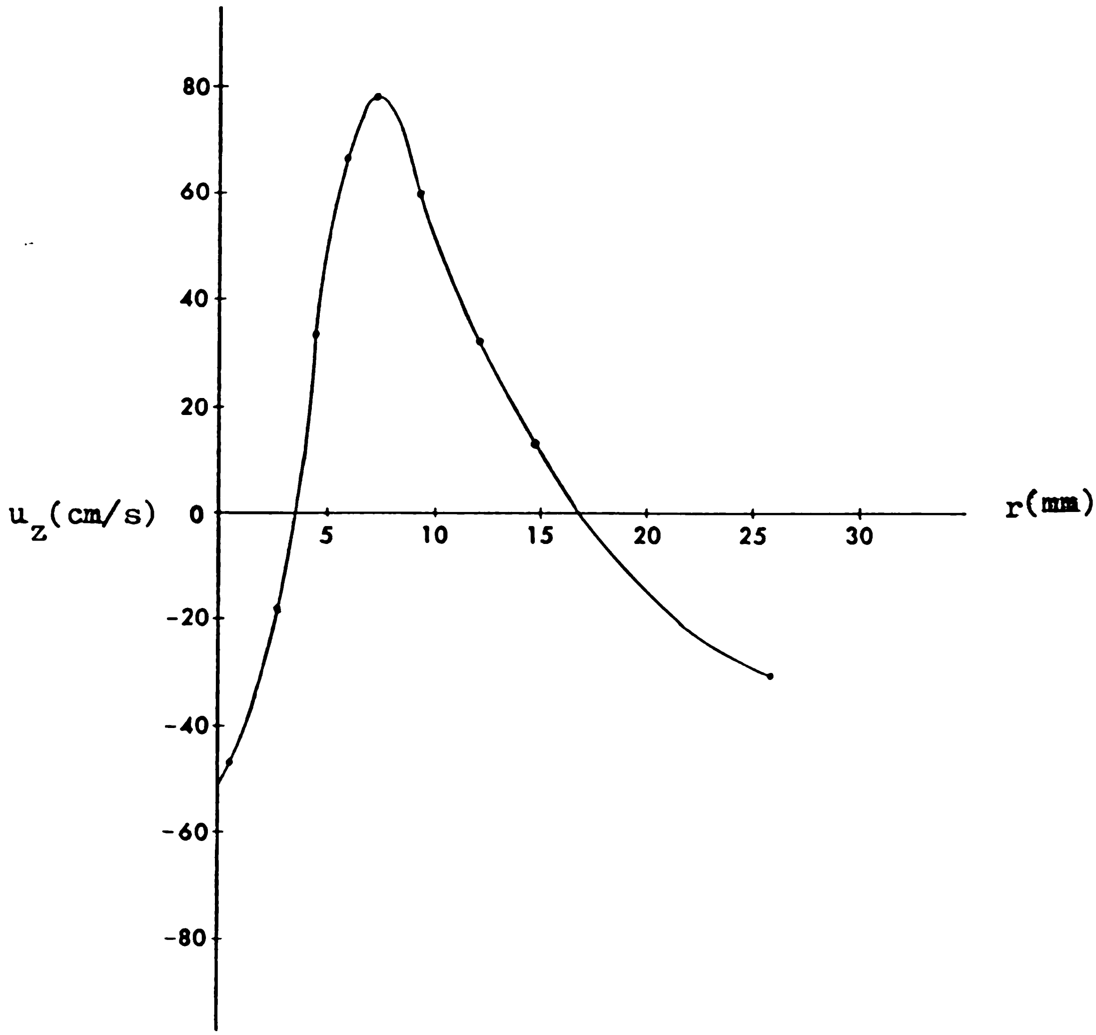

Figure C.2 . Axial velocity measurements.

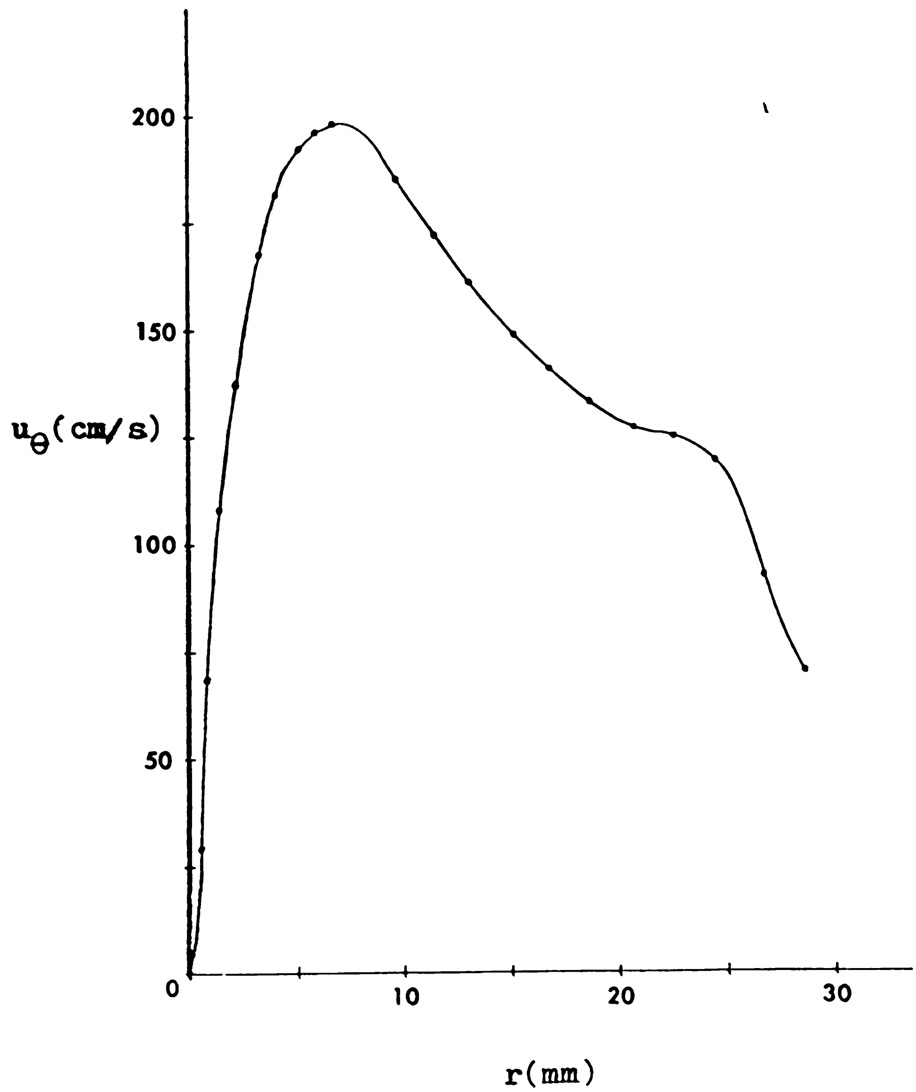

Figure C.3 . Tangential velocity measurements.

REFERENCES

Adrian, R. J., and Fingerson, L. M., 1981, TSI Short Course.

Atkins, P. W., 1978, Physical Chemistry, W. H. Freeman & Co.

Boadway, J. D., and Karahan, E., Feb. 1981, "Corrections of Laser Doppler Anemometer Readings for Refraction at Cylindrical Interfaces", DISA Information: Measurement and Analysis, No. 26, p. 4.

Boadway, J. D., Feb. 1983, "Corrections of Laser Doppler Anemometer Readings for Refraction at Cylindrical Interfaces", DISA Information: Measurement and Analysis, No. 28, p. 31.

Born, M., and Wolf, E., 1959, Principles of Optics, Pergamon Press Inc.

Bradley, D. and Pulling, D. J., 1959, "Flow Patterns in the Hydraulic Cyclone and Their Interpretation in Terms of Performance", Trans. Instn. Chem. Engrs., 37, p. 34.

Cheung, T. K., and Koseff, J. P., Feb. 1983, "Simultaneous Backward-scatter Forward-scatter Laser Doppler Anemometer Measurements in an Open Channel Flow", DISA Information: Measurement and Analysis, No. 28, p. 3.

Crosignani, B., DiPorto, P., and Bertolotti, M., 1975, Statistical Properties of Scattered Light, Academic Press, Inc.

Dabir, B., 1983, "Mean Velocity Measurements In A 3"-Hydrocyclone Using Laser Doppler Anemometry", Ph.D. Thesis, Michigan State University.

DISA Electronics, August 1972, "DISA Type 55L Laser Doppler Anemometer", Leaflet No. 2005/E.

DISA Electronics, 1978, "Laser Anemometer Equipment Catalog", Publ. No. 8208E.

Durrani, T. S., and Greated, C. A., 1977, Laser Systems in Flow Measurement, Plenum Press.

Durst, F., Melling, A., and Whitelaw, J. H., 1976, Principles and Practice of Laser-Doppler Anemometry, Academic Press.

Durst, F., Keck, T., and Kleine, R., 1981, "Turbulence Quantities and Reynolds Stress In Pipe Flow of Polymer Solutions Measured", Turbulence In Liquids, University of Missouri-Rolla.

Durst, F., September 1982, "REVIEW-Combined Measurements of Particle Velocities, Size Distributions, and Concentrations", Tansactions of the ASME - Journal of Fluids Engineering, 104, p. 284.

Halliday, D., and Resnick, R., 1974, Fundamentals of Physics, John Wiley & Sons, p. 669.

Kelsall, D. F., 1952, "A Study of the Motion of Solid Particles in a Hydraulic Cyclone", Trans. Instn. Chem. Engrs., 30, p. 87.

Knowles, N. S. R., 1971, "Photographic Fluid Velocity Measurement in a Hydrocyclone", M. Eng. Thesis, Dept. of Chem. Eng., McMaster University, Hamilton, Ontario.

Mie, G., 1908, Ann. d. Physik, 25 (4), p. 377.

Rietema, K., 1961a-d, "Performance and Design of Hydrocyclones -- I, II, III, IV", Chem. Eng. Sci., 15, p. 298, 303, 310, 320.

Rossi, B., 1957, Optics, Addison-Wesley Publishing Co., Inc., p. 366.

Rudd, M. J., 1969, "A New Theoretical Model for the Laser Dopplermeter", Journal of Scientific Instruments (Journal of Physics E), Series 2, 2, p. 55.